

Report

Project No. 33486

Neutron Absorber Material Corrosion Testing Final Report

Tedd E. Lister
Ronald E. Mizia
Luis A. Diaz
Michael G. Jones
Henry C. Hutcheson




The INL is a U.S. Department of Energy National Laboratory
operated by Battelle Energy Alliance.

Idaho National Laboratory

**Neutron Absorber Material Corrosion
Testing Report**

Identifier:		
Revision:	0	
Effective Date:	12/17/2020	Page: 1 of 52

Prepared by:




Tedd E. Lister

12/17/2020

Date

Approved by:



Joshua Jarrell

12/17/2020

Date

Neutron Absorber Material Corrosion Testing Report	Identifier: Revision: 0 Effective Date: 12/17/2020
---	--

Page 3 of 52

Acronyms

ASTM –	ASTM International
ANA –	Advanced Neutron Absorbing Alloy
BB –	Bohler Bleche
BSS –	borated stainless steel
CarTech –	Carpenter Technology Corporation
CPP –	cyclic potential polarization
DOE –	Department of Energy
E_{corr} –	corrosion potential
E_{pit} –	pitting potential
E_{rp} –	repassivation potential
INL –	Idaho National Laboratory
LLNL –	Lawrence Livermore National Laboratory
LPR –	linear polarization resistance
NAM –	neutron absorbing material
NSNFP –	National Spent Nuclear Fuel Program
NRC –	Nuclear Regulatory Commission
ORNL –	Oak Ridge National Laboratory
OCRWM –	Office of Civilian Radioactive Waste Management
RO –	reverse osmosis
SNF –	spent nuclear fuel
SNL –	Sandia National Laboratory
SAM –	structurally amorphous materials
SS –	stainless steel
WPOB –	waste package outer barrier

Idaho National Laboratory**Neutron Absorber Material Corrosion
Testing Report**

Identifier:

Revision: 0

Effective Date: 12/17/2020

Page 4 of 52

1. Introduction

Neutron absorbing materials (NAMs) are used within commercial spent nuclear fuel (SNF) canisters to maintain nuclear subcriticality in storage. Including NAMs within commercial SNF canisters absorbs neutrons and thereby reduces the potential for criticality events. For the FY2020, Idaho National Laboratory (INL) was tasked with reviving the corrosion testing portion of a neutron absorber development program supported by the National Spent Nuclear Fuel Program (NSNFP) and later by the Office of Civilian Radioactive Waste Management (OCRWM). Previous work focused on two classes of materials: commercially produced borated stainless steels (BSSs) and INL-developed nickel-based alloys with gadolinium added as a neutron absorber. This report will provide results from corrosion testing performed during FY2020. The testing was performed according to INL PLN-6095, which was formulated through consensus with staff at Oak Ridge National Laboratory (ORNL), Sandia National Laboratory (SNL), and INL [1].

1.1 Testing approach

Corrosion evaluations are inherently difficult, presenting many challenges and limitations. When possible, examination using in-service conditions is the best approach. However, in the problem being faced pertaining to long-term SNF storage, neither the service conditions nor the vast service time required can be replicated. This has posed a challenge in predicting the long-term behavior of materials used in repositories. The approach used in assessing NAMs leverages the electrochemical testing scheme previously employed in developing a comprehensive corrosion model [2].

Corrosion can be categorized into two broad types: general (uniform) corrosion and localized corrosion. The approach taken in this work is to examine both types. General corrosion is a relatively uniform process in which the metal is reduced in thickness. This can be ascribed a linear rate, such as millimeters per year (mmpy). For engineered structures, the environmental conditions across all surfaces vary and thus may not appear uniform when viewed macroscopically. Localized corrosion is much more challenging and potentially damaging compared to general corrosion. Localized corrosion is a general term for several types (mechanisms) of corrosion that attack at specific places on surfaces. Such attacks can be driven by microstructural and physical aspects of the engineered structure, as well as by the localized environment. Alloys tend to have non-uniform compositions (such as secondary phases, welds, and grain boundaries) that may result in areas with greater susceptibility to localized corrosion. Environmental factors such as crevices (where surfaces are held against other surfaces) can limit the free diffusion of chemicals from the surface and result in corrosive conditions. Galvanic effects are also

Neutron Absorber Material Corrosion Testing Report	Identifier: Revision: 0 Effective Date: 12/17/2020
---	--

Identifier: Revision: 0 Effective Date: 12/17/2020	Page 5 of 52
--	--------------

possible, with dissimilar metals in ohmic contact interacting such that one of the metals acts as the corroding anode.

Pitting corrosion, the most common form of localized corrosion, is often described as having an initiation event followed by a growth phase [3]. The initiation event is the birth of a pit, which may or may not transition to growth and may involve significant latency. The growth phase occurs as the initiated pit continues to oxidize metal at the site. The growth may continue or repassivate, with oxide reforming over the metal.

The testing protocol employed in this work was based on those used previously to model waste package outer barrier (WPOB) corrosion [2]. An electrochemical test sequence based on these evaluations was used to evaluate both localized and general corrosion [4]. General corrosion was assessed using linear polarization resistance (LPR). The magnitude of the current (slope) near E_{corr} is proportional to the general corrosion rate [5]. A more challenging assessment is that for localized corrosion. Electrochemical tests were used to determine three important potentials: (1) E_{corr} , (2) pitting potential (E_{pit}), and (3) repassivation potential (E_{rp}). These parameters are described in more detail in Section 1.2 below. The localized corrosion model for the WPOB employed electrochemical testing to determine these parameters. For evaluation purposes, numerical models were built for both E_{corr} and E_{rp} , based on varying ion composition and temperature [2]. This work will not develop a comprehensive environmental model, as it is more of a comparative materials evaluation using three solutions at one temperature, with seawater considered the most relevant condition.

1.2 Testing methods

E_{corr} is a mixed potential in that it is set by a balance of anode and cathode reactions occurring on the specimen surface. For most service conditions, corrosion is not driven externally (except by galvanic corrosion driven by the differential potential of two metals); thus, by definition, it occurs at E_{corr} . The cathode reaction is either O_2 reduction or H_2 production, depending on the specimen and environment. In general, as the anode corrosion increases, the observed potential shifts negative as the cathode reaction increases. A transient behavior is observed when the driving force for corrosion is at the edge of stability, resulting in alternating corrosion-passivation events. In the case of localized corrosion, this could be driven by a single pit or behavior distributed across the surface.

Cyclic potential polarization (CPP) tests were performed following the LPR tests. The CPP tests provide an understanding of the specimen's corrosion and electrochemical characteristics in the tested environment as a function of potential. Figure 1 shows a diagram of a CPP curve for a metal that is

Idaho National Laboratory

Neutron Absorber Material Corrosion Testing Report	Identifier: Revision: 0 Effective Date: 12/17/2020
---	--

Neutron Absorber Material Corrosion Testing Report	Identifier: Revision: 0 Effective Date: 12/17/2020
---	--

Page 6 of 52

susceptible to pitting corrosion. For most metals and alloys, the electrochemical response can be broken down into three regions: the active region, the passive region, and the pitting region. The current is plotted as an absolute value in log scale. The active region is centered around E_{corr} , which is defined by a complex balance of chemical reactions that sets the potential relative to a reference electrode. It is the point where currents for these reactions are balanced—such that, when the potential is manipulated (using a potentiostat and electrochemical cell), the net current increases in either direction. The scan is initiated negative of the measured E_{corr} in the positive direction. After passing through E_{corr} (note that, in this study, we report E_{corr} with air purge and not based on the CPP curve), the net current flips from cathodic to anodic, and, depending on the environment, a broad hump may be observed which is the anodic dissolution of the metal in what is called the “active” region. This peak often decreases as the oxide layer reforms in the passive region, the oxide layer being stabilized by the more positive potential. In relatively benign environments (for the metal/alloy), the current in the active region may be very small, without a defined peak. The current will eventually increase in the passive region, either due to pitting corrosion or, in some cases, transpassive corrosion (often more positive in non-pitting alloy/environment conditions). The initiation of pitting corrosion is often preceded by noise spikes in current, due to pit initiation and repassivation before stable pitting sets in. Deeper into the pitting region, the current increases, and the sweep is reversed at the switching potential. If pitting has initiated on the specimen, the current will remain high on the return sweep until the potential is insufficient to sustain the pitting. E_{rp} is a potential assigned to describe when pits have repassivated on the return sweep. Going back to the switching potential, if the current decreases quickly and closely follows the forward sweep, it is likely the specimen is not susceptible to localized corrosion under the tested conditions. In that case, the current observed is either oxide film growth or transpassive corrosion. The remainder of the sweep may show features similar to the forward sweep. Once the potential reaches the starting potential, the test is stopped.

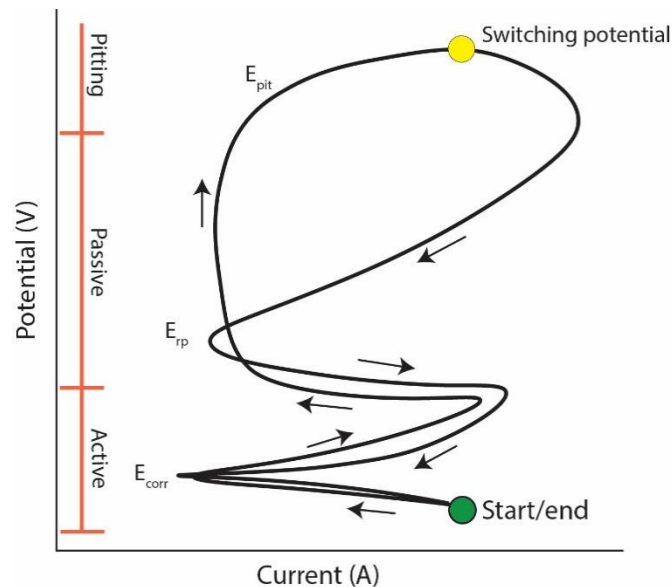


Figure 1. Diagram of a generic CPP curve.

Two important parameters are obtained from the curves: the pitting potential (E_{pit}) and E_{tp} . E_{pit} is defined as the point at which a sharp increase in current is observed in the forward sweep, where pitting is initiated. E_{tp} is defined as the point at which the current from pitting has subsided—typically the point at which the current switches sign (net current is negative) or crosses the forward sweep. This would indicate the point at which the material is defined as being stable (to pitting corrosion). Stability is assessed by comparing measured E_{tp} to E_{corr} , where the more positive E_{tp} is relative to E_{corr} , the less likely pitting corrosion will occur. Conversely, if E_{corr} is similar to or more positive than E_{tp} , the alloy and environment are considered incompatible, as localized corrosion is likely to occur. This was the basis for evaluating Alloy 22 as a WPOB material, with a parameterized model formulated and used to predict crevice corrosion [2].

While the approach to evaluating corrosion bears similarities to previous corrosion evaluations, the goals of this work are quite different. NAMs are not considered for containment; thus, there is a slightly lower functional requirement for the material. The NAMs are likely to experience some localized damage if they remain largely intact and functioning to reduce criticality. Note that, as the material is likely to be exposed on both sides, the impact is doubled and must be factored into the design. This work is a materials selection activity that examines a small number of conditions for several different alloy types. Benchmark (non-NAM) alloys are included for comparison in order to leverage existing knowledge of their corrosion properties.

Neutron Absorber Material Corrosion Testing Report	Identifier:
	Revision: 0
	Effective Date: 12/17/2020

Page 8 of 52

1.3 Testing environments

Aqueous corrosion is highly influenced by ion species and concentration. Chloride ions are known to promote localized corrosion of many forms, including pitting. A significant body of work centers around the stability of metals in chloride environments, particularly seawater. While chloride is known to promote corrosion, other ions such as nitrate and sulfate act as inhibitors of pitting corrosion. The basis condition for this work is seawater, a universal concentrated water [6]. Table 1 shows the top three anion components for seawater, indicating that chloride dominates the composition, followed by sulfate and carbonate. The ionic composition of seawater is much higher than that used previously for NAM testing, in which the total ionic content was 0.0045–0.0075 M [7].

Table 1. Anion composition of seawater [8].

Ion	Con (g/Kg)	Con (mol/kg)
chloride	19.353	0.54588
sulfate	2.701	0.0281
carbonate	0.142	0.00233

Testing was performed at 30°C using non-creviced specimens for initial evaluation and to provide data for making decisions as to what materials to select for further evaluation. Two other solutions were also tested: 0.028 M NaCl and 0.1 M HCl. The former was derived from a chloride solution used in testing funded by the National Regulatory Commission (NRC) and the Department of Energy (DOE) for assessing Alloy 22 [9-10]. The HCl solution can be viewed as a low-pH environment such as could be generated at a crevice. Both 0.028 M NaCl and 0.1 M HCl were used in INL testing of NAM materials [11].

2. Experimental

Testing was performed using ASTM G5 as a guide [12]. Experiments were performed according to step-by-step procedures, with checklists to ensure consistency. These checklists are companions to the laboratory notebooks that fully document the testing. The two testing stations are labeled to prevent identification issues. Tests were staggered to prevent specimens from being switched, as ID markings are not present on the specimens.

2.1 Specimens

The following alloy types were tested: Type 304L stainless steel (SS), Type 316L SS, 304B4 SS, 304B5 SS, Alloy 22, M326 (low Cr) Advanced Neutron Absorber (ANA) and M327 (high Cr) ANA. The

Idaho National Laboratory

Neutron Absorber Material Corrosion Testing Report	Identifier:
	Revision: 0
	Effective Date: 12/17/2020

Page 9 of 52

material compositions are shown in Table 2 below, as obtained from heat papers or through analyses performed in previous testing programs. Types 304L and 316L SS were obtained from Metal Samples Company, finished to 600 grit SiC. Alloy 22 specimens were also obtained from Metal Samples Company. ANA (also called Ni-Cr-Mo-Gd) specimens were remaining materials either machined by Metal Samples Company or the INL machine shop, finished to 600 grit SiC. BSS were those specimens remaining from previous testing activities.

Table 2. Composition of alloys used in this testing.

Material	ANA	ANA	Alloy 22	304B4	304B5	304L	316L
Heat	M326	M327	2277-7-3130	182194	182195	D88180A	AZ608
Nickel	Bal	Bal	Bal	13.39	13.39	8.41	10.5
Iron	0.025	0.032	3.54	Bal	Bal	Bal	Bal
Chromium	14.71	21.01	21.55	19.46	19.36	18.27	16.57
Molybdenum	14.53	14.32	13.47			0.33	2.018
Gadolinium	2	1.98					
Boron				1.17	1.32		
Oxygen	0.0032	0.0042					
Nitrogen						0.069	0.034
Phosphorus			0.007			0.022	0.03
Manganese	0.001	0.01	0.25	1.91	1.84	1.64	
Magnesium	0.002	0.002					
Cobalt	0.009	0.003	0.74			0.12	0.21
Carbon	0.006	0.001	0.003	0.05	0.05	0.02	0.022
Silicon	0.013	0.018	0.024			0.44	0.27
Sulfur	0.001	0.002	0.004			0.024	0.0215
Copper						0.35	0.31
Vanadium			0.12				
Tungsten			2.83				

The specimens were of the boldly exposed type (no intentionally designed crevices), with cylinders 1.7 in. in length and 0.25 in. in diameter attached to a threaded rod. The rod was isolated from contact with the solution by a glass tube with a flat Viton gasket sealing the submerged interface. For 304B4 and 304B5, crevice specimens were employed, as they were the only available specimens and material of that specification does not exist. The specimens were 0.75-in. x 0.75-in. x 0.375-in. blocks with a 0.325-in. through hole machined into the larger area surfaces. These specimens were tested without crevice assemblies. Teflon gaskets were used as seals between the glass and the specimen. The 304B5 specimens were refinished test specimens from previous work, as no untested specimens existed. Specimens were

Idaho National Laboratory**Neutron Absorber Material Corrosion
Testing Report**

Identifier:

Revision: 0

Effective Date: 12/17/2020

Page 10 of 52

cleaned by being rinsed sequentially in acetone, ethanol, and deionized water to remove grease and other detritus prior to testing. The specimens were weighed on a 5-place balance both before and after testing. To assess ANA specimens in some tests, specimens were pickled in 1 M HCl in a small beaker at room temperature. Specimens tested in seawater were pickled for nine days, while the M327 tested in 0.1 M HCl was pickled for 29 days.

2.2 Solution preparation

Three solutions are included in this work: artificial seawater (referred to simply as seawater), 0.028 M NaCl, and 0.1 M HCl. The solutions were made using American Chemical Society (ACS)-grade chemicals. A calibrated three-place balance was used to weigh the chemicals. These weights were recorded in laboratory notebooks and/or datasheets. Water was obtained via the reverse osmosis (RO) purification system, fed by a building RO water system. The final water conductivity was 18 MΩ-cm. The solution volume for the tests was 900 mL. ASTM D1141 was used as a guide for producing artificial seawater [8].

2.3 Electrochemical cell

The electrochemical cell was based on ASTM G5 specifications [12]. The cell and associated accessories were made of borosilicate glass. The cell has facilities for gas purging through a ceramic frit (150 cm³/min). A glass condenser, through which gas exited the cell, was employed to reduce water evaporation during the test. All tests were performed at 30°C. The temperature was set through a thermocouple-controlled heating mantle. Thermocouples were checked for tolerance at INL calibration labs. A graphite rod was used as the counter electrode and was cleaned and/or replaced regularly. Commercially sourced (Pine Instruments) reference electrodes of the Ag/AgCl (4 M KCl) type (0.199 V vs. normal hydrogen electrodes) were compared to two reference electrodes (of the same type and source) set aside specifically as standards.

2.4 Electrochemical testing sequence:

Electrochemical testing was performed using a prescribed sequence that (1) measures E_{corr} with air purge, (2) measures E_{corr} with N₂ purge while removing the oxygen from Step 1, (3) performs three linear polarization resistance (LPR) tests, and (4) performs a CPP test from 0.2 V negative of the measured E_{corr} in N₂. LPR tests were performed by stepping from E_{corr} by -30 mV and sweeping positive 60 mV (a sweep of ±30 mV of E_{corr}). ASTM G59 was used as a basis for designing the tests [5]. For CPP, the anodic switching potential varied with specimen type, with SSs displaying excessive pitting if swept too far

Idaho National Laboratory

Neutron Absorber Material Corrosion Testing Report	Identifier:
	Revision: 0
	Effective Date: 12/17/2020

Identifier: Revision: 0 Effective Date: 12/17/2020	Page 11 of 52
--	---------------

positive in comparison to nickel-based alloys. The scan rate for LPR and CPP testing was 0.6 V/hr (0.167 mV/sec).

2.5 Post-test analysis

Data was analyzed using software included with the potentiostat. Specific calculations for corrosion rates were based on guidelines obtained from ASTM G102 [13]. The corrosion rate was calculated using EC-Lab software (Version 11.34) provided with the BioLogic potentiostat. For CPP curve analysis, the final E_{corr} in air provides a value for where the alloy potential resides in equilibrium with air. The pitting potential (E_{pit}) was estimated as the potential where the current rapidly increases, and the E_{rp} was estimated as being the value at which the reverse sweep crossed zero current (switching from positive to negative). For SS specimens, this was not always observed, and the E_{rp} was chosen as the value at which a sharp deviation in the current drop on the return sweep occurred. Specimens were weighed both before and after testing, and the differences were reported. No attempt was made to descale specimens, and visually significant scaling was not observed.

2.6 Specimen and solution analysis

Several methods of post-test analysis have been employed: photography, optical microscopy, and scanning electron microscopy. Measurement of pit depths was also performed for some specimens, using an optical microscope with a z-calibrated motor. In the future, specimens will be available to perform other analysis methods, as deemed useful to interpret results. A volume of test solution was also captured and will be kept for possible future analysis, to be performed when deemed useful to interpret results.

3. Results

3.1 Corrosion testing results

3.1.1 E_{corr} test results

The E_{corr} of specimens in solutions purged with air was measured for 4 hours, and the last value was recorded. In the event of a sharp transient response at the end of the measurement, the value prior to the final point was selected in order to be more representative of the E_{corr} . This value places the equilibrium potential in an air-saturated solution. E_{corr} was determined from E_{corr} curves and is presented with the CPP data in Table 4.

3.1.1.1 E_{corr} in seawater

The E_{corr} curves for SS in seawater are shown in Figure 2. Both 304L and 304B4 show several negative-going transients, an indicator of localized corrosion [14], while the 316L specimen is mostly smooth. This

Neutron Absorber Material Corrosion Testing Report

Identifier:

Revision: 0

Effective Date: 12/17/2020

Page 12 of 52

agrees with the known performance differences between 304L and 316L, where the Mo containing 316 alloy is often selected over 304 in marine environments [15]. The curve for 304B5 shows some transient activity early on, but a smooth curve thereafter.

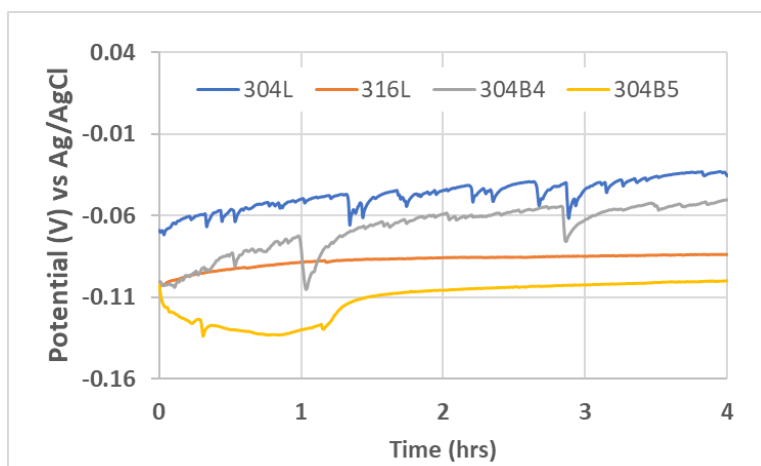


Figure 2. E_{corr} traces for SS alloys in seawater.

Figure 3 shows E_{corr} curves for nickel-based alloys in seawater. Alloy 22 has a smooth curve, while the ANA specimens both show transient responses indicative of localized corrosion. Previous work identified the secondary phase as possessing poor corrosion characteristics [16]. The Ni_5Gd secondary phase selectively dissolves, as its low Cr level prevents it from forming an effective passive film. ANA specimens that were pickled prior to testing show much smoother traces.

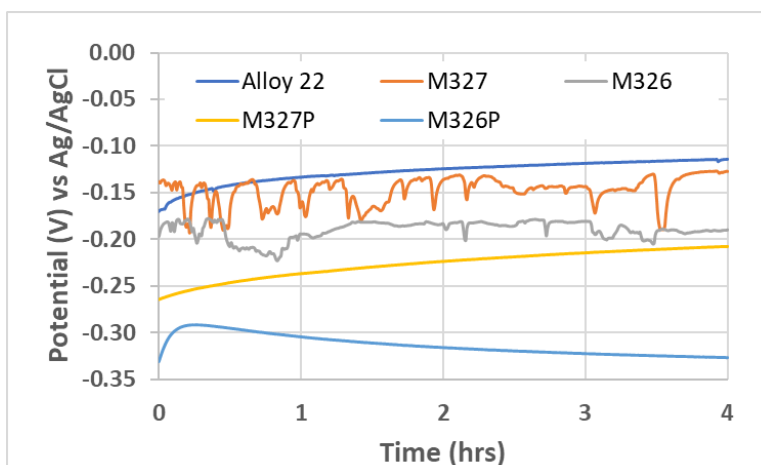


Figure 3. E_{corr} traces for nickel-based alloys in seawater. The “P” suffix denotes specimens pickled prior to testing.

Neutron Absorber Material Corrosion Testing Report

Identifier:

Revision: 0

Effective Date: 12/17/2020

Page 13 of 52

3.1.1.2 E_{corr} in 0.028 M NaCl

Figure 4 shows E_{corr} measurements in 0.028 M NaCl. Transients are present for all specimens except 316L. The transients are smaller than observed for seawater, likely due to the reduced chloride composition lowering corrosivity.

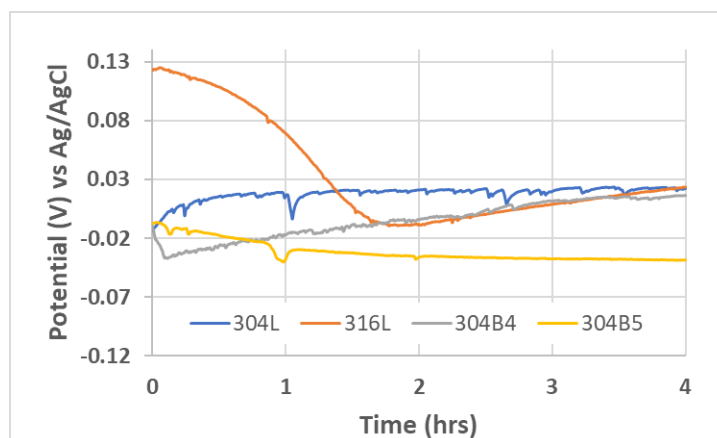


Figure 4. E_{corr} traces for SS alloys in 0.028 M NaCl.

Figure 5 shows E_{corr} measurements in 0.028 M NaCl. Alloy 22 shows a smooth E_{corr} trace. The ANA specimens show small transients relative to those observed in seawater (Figure 3).

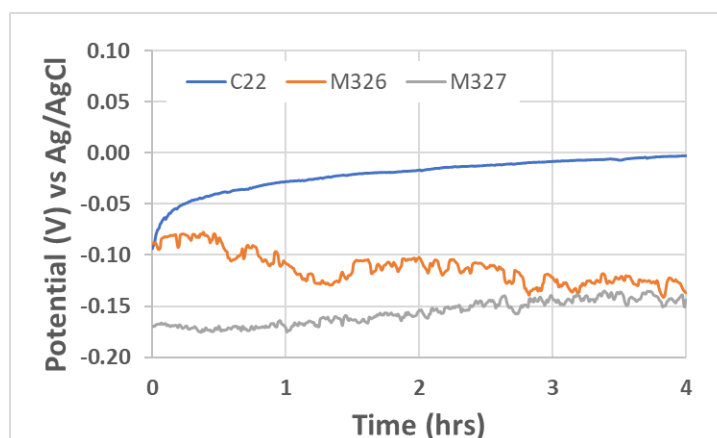


Figure 5. E_{corr} traces for nickel alloys in 0.028 M NaCl.

3.1.1.3 E_{corr} in 0.1 M HCl

Figure 6 shows E_{corr} measurements for SS specimens in 0.1 M HCl. There is a bifurcation between specimens, with the 316L and 304L specimens (after 1 hour) showing values similar to those measured in seawater and NaCl. The BSS specimens (and the 304L in the initial hour) are approximately 0.25 V more

Neutron Absorber Material Corrosion Testing Report

Identifier:

Revision: 0

Effective Date: 12/17/2020

Page 14 of 52

negative and essentially lay on top of each other after ~0.5 hr. The more negative potential is likely due to active corrosion without repassivation; the stable potential is explained by the lack of initiation/passivation events.

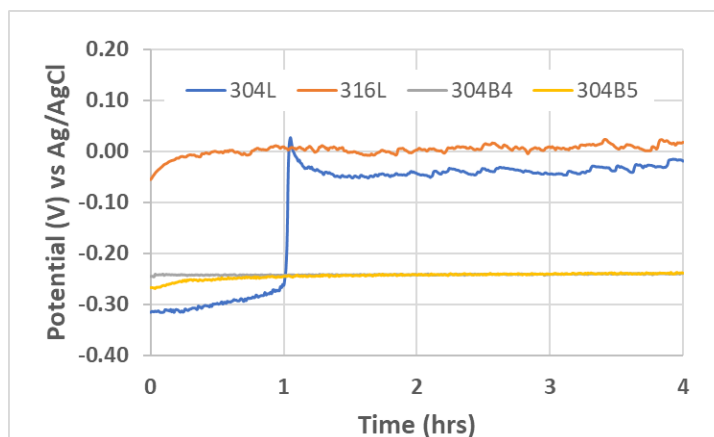


Figure 6. E_{corr} traces for SS alloys in 0.1 M HCl.

Figure 7 shows E_{corr} traces for nickel alloys in 0.1 M HCl. The corrosion potential for Alloy 22 is quite positive, while those for the ANA specimens are significantly more negative. All traces are quite smooth; in the case of Alloy 22, there is no corrosion, while ANA specimens are actively corroding, likely confined to the secondary phase. After pickling, the M327 specimen showed an increase in E_{corr} , reaching similar values as those displayed by Alloy 22. The lack of transients in the unpickled ANA specimens could be due to the secondary phase being in an unchanging dissolution condition in which the oxide film was unstable (no passivation through oxide formation), as opposed to a situation in which the oxide film stability switches, resulting in a varying surface condition.

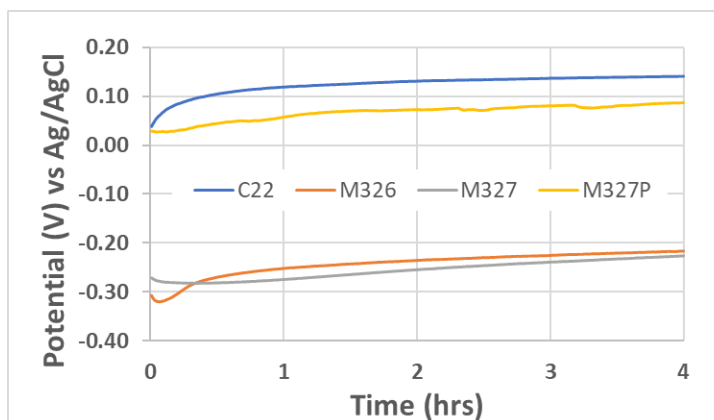


Figure 7. E_{corr} traces for nickel alloys in 0.1 M HCl. The “P” suffix denotes specimens pickled prior to testing.

Idaho National Laboratory

Neutron Absorber Material Corrosion Testing Report	Identifier:
	Revision: 0
	Effective Date: 12/17/2020

Page 15 of 52

3.1.2 LPR test results

For each test, three LPR sweeps were performed to measure the general corrosion rate. Table 3 shows the average corrosion rates obtained during testing. For cases in which LPR data were not recorded, it is thought that localized corrosion interfered with the LPR current measurement. In these tests, measured E_{corr} values contained signatures of pitting corrosion, with a decrease in potential during pitting and metastable pitting events [14]. Specimens generally demonstrate low corrosion rates for 0.028 M NaCl and seawater, but the rates are several orders of magnitude higher for 0.1 M HCl. Alloy 22 is the exception, showing less than an order of magnitude increase in corrosion rates when in 0.1 M HCl.

Table 3. General corrosion rates calculated from LPR testing.

Date	Alloy	Solution	Rate (mmpy)	SD (mmpy)
7/27/2020	Alloy 22	0.028 M NaCl	7.94E-06	5.76E-07
10/30/2020	Alloy 22	0.028M NaCl	1.71E-05	1.10E-05
8/6/2020	M327	0.028 M NaCl	1.15E-04	3.71E-05
8/19/2020	M327	0.028 M NaCl	4.74E-05	4.18E-06
8/11/2020	M326	0.028 M NaCl	-	-
8/17/2020	M326	0.028 M NaCl	9.64E-04	2.67E-04
8/21/2020	M326	0.028 M NaCl	1.25E-05	3.91E-07
7/29/2020	316L	0.028 M NaCl	9.20E-05	1.64E-05
8/3/2020	304L	0.028M NaCl	-	-
10/28/2020	316L	0.028 M NaCl	3.66E-05	2.79E-06
10/27/2020	304L	0.028 M NaCl	1.08E-05	1.19E-05
8/26/2020	304B4	0.028 M NaCl	1.22E-05	4.64E-06
9/4/2020	304B4	0.028 M NaCl	1.74E-04	9.90E-05
9/8/2020	304B5	0.028 M NaCl	-	-
7/28/2020	Alloy 22	Seawater	4.19E-06	3.53E-07
9/22/2020	Alloy 22	Seawater	8.84E-06	2.83E-06
8/7/2020	M327	Seawater	-	-
8/25/2020	M327	Seawater	-	-
8/26/2020	M327	Seawater	4.66E-05	2.15E-05
11/12/2020	M327P	Seawater	1.52E-05	3.57E-06
8/12/2020	M326	Seawater	6.93E-06	9.56E-07
8/20/2020	M326	Seawater	1.87E-05	7.87E-07
11/13/2020	M326P	Seawater	3.84E-03	3.69E-04
7/30/2020	316L	Seawater	2.38E-06	5.70E-07
9/2/2020	316L	Seawater	9.20E-06	1.54E-06
8/4/2020	304L	Seawater	-	-

Idaho National Laboratory

Neutron Absorber Material Corrosion
Testing Report

Identifier:

Revision: 0

Effective Date: 12/17/2020

Page 16 of 52

9/15/2020	304L	Seawater	6.91E-06	1.79E-06
9/3/2020	304B4	seawater	1.14E-05	1.06E-06
9/9/2020	304B5	Seawater	2.58E-04	2.79E-05
7/29/2020	Alloy 22	0.1 M HCl	2.02E-05	3.17E-06
11/9/2020	Alloy 22	0.1M HCl	1.96E-05	3.43E-06
8/10/2020	M327	0.1M HCl	1.15E-01	2.15E-02
8/21/2020	M327	0.1M HCl	1.42E-02	2.98E-03
11/5/2020	M327P	0.1M HCl	4.61E-05	1.16E-05
8/13/2020	M326	0.1M HCl	-	-
8/18/2020	M326	0.1M HCl	4.33E-01	8.89E-02
8/27/2020	M326	0.1M HCl	5.57E-02	3.36E-03
7/30/2020	316L	0.1 M HCl	2.19E-02	1.58E-03
11/5/2020	316L	0.1M HCl	9.91E-03	6.64E-04
8/5/2020	304L	0.1 M HCl	1.41E-04	1.43E-04
11/5/2020	304L	0.1M HCl	2.26E-04	5.23E-05
8/27/2020	304B4	0.1M HCl	6.81E-02	1.78E-02
9/10/2020	304B5	0.1M HCl	4.72E-02	1.08E-02

*mmpy: millimeters per year**SD: standard deviation (3 measurements)*

Summary for 0.028 M NaCl: All specimens showed similar general corrosion rates centered between 1×10^{-5} to 1×10^{-6} mmpy. The ANA specimens showed slightly higher rates compared to SS, while Alloy 22 showed rates of about an order of magnitude lower than SS. The BSS specimens saw rates similar to those of conventional SS specimens.

Summary for seawater: Very similar to what was observed for 0.028 M NaCl. The outlier for acid-pickled M326 is noted and deserves further study, as we suspect that the acid pickling was insufficient.

Summary for 0.1 M HCl: General corrosion rates were about 3–4 orders of magnitude higher for all specimens apart from Alloy 22, for which an increase of only about one order of magnitude was observed. The rate for pickled ANA approached that of Alloy 22.

3.1.3 CPP test results

3.1.3.1 CPP results in seawater

CPP curves for 304L and 316L are shown in Figure 8, with the values for the CPP parameters labeled. Note that while E_{corr} (under N_2 purge) is labeled in Figure 8, the tabulated values shown later (Table 4) are from the E_{corr} plots under air purge shown above (Figures 2-7). The forward curve (positive scan direction) starts at a potential negative of the measured E_{corr} (under N_2 purge) value and, for both alloys,

Neutron Absorber Material Corrosion Testing Report

Identifier:

Revision: 0

Effective Date: 12/17/2020

Page 17 of 52

displays a response typical of chloride-containing solutions: on the forward sweep, small transients are observed approaching E_{pit} , followed by a rapid increase in current. E_{pit} is significantly more positive for 316L. On the return sweep, the current is sustained such that it exceeds (hysteresis) that of the forward sweep. The increased current is due to active pit dissolution. This positive (anodic) current eventually declines as the oxide film reforms on the surface of the formed pits. A change in current from anodic to cathodic was not observed, leaving the estimation of E_{rp} somewhat vague. E_{rp} was selected to be the point at which the current stabilized on the return sweep, as labeled in Figure 8. While 316L displayed a drop in current that was greater in magnitude compared to 304L, the actual E_{rp} values were not significantly different, demonstrating the value of comparing curves vs. relying on specific values.

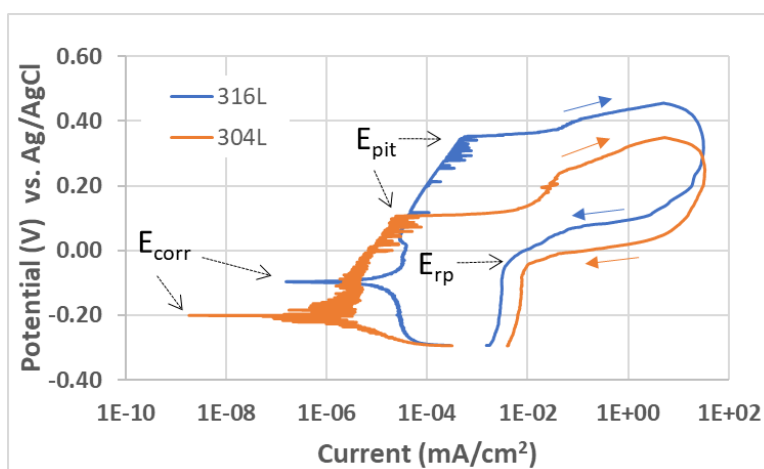


Figure 8. CPP curves for Types 304L and 316L SS in seawater.

Figure 9 shows CPP plots for the two BSS specimens in seawater. In the forward sweep, 304B5 shows a higher E_{pit} value, despite having a higher B content (1.17 vs. 1.32 wt.%). This was observed when previously comparing these two alloys (of the same material as was used here) in dilute chloride/sulfate/nitrate-containing solutions [17]. There is greater variation in current prior to E_{pit} than for the benchmark alloys referenced in Figure 8. On the return sweep, significant hysteresis is observed for both specimens, featuring an E_{rp} value very similar to those observed for 304L and 316L specimens, with 304B5 being only slightly more negative. Again, the current did not change sign, similar to what was observed in Figure 8.

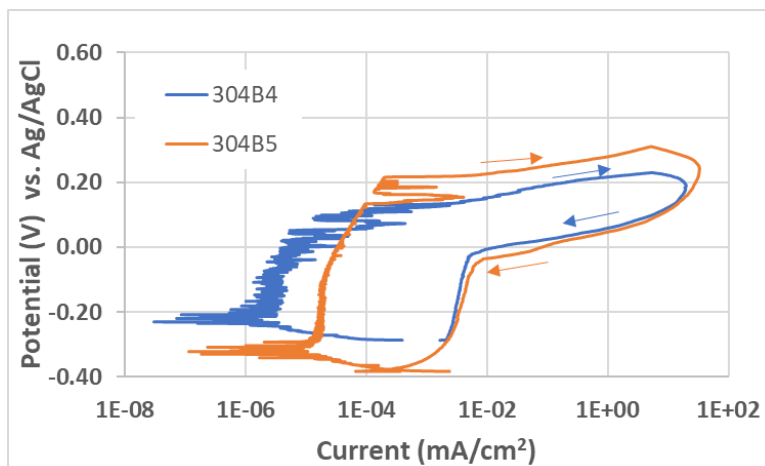


Figure 9. CPP curves for 304B4 and 304B5 alloys in seawater.

The curve for Alloy 22 is presented in Figure 10. The Alloy 22 specimen showed a low current and no evidence of pitting corrosion, as evidenced by the lack of hysteresis in the return sweep. Alloy 22 possesses well-known stability in high-chloride environments, where it is considered “practically immune to pitting corrosion” [4].

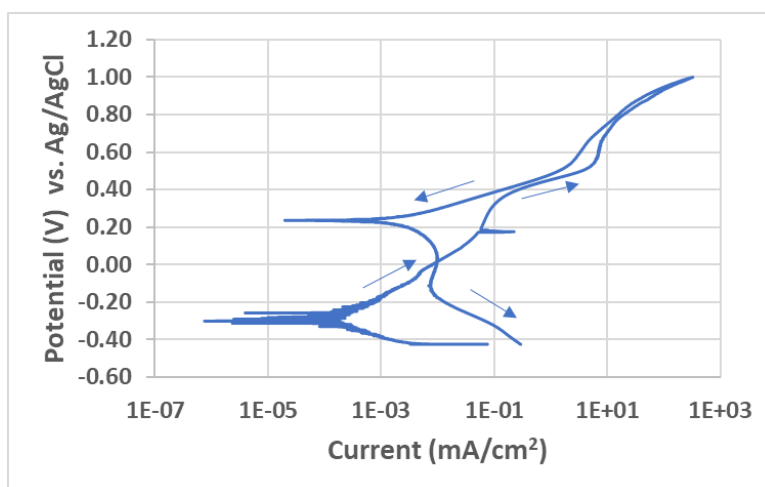


Figure 10. CPP curves for Alloy 22 in seawater.

Curves for the two ANA specimens are shown in Figure 11. Compared to Alloy 22, both ANA specimens show significantly higher current in the passive region. On the return sweeps, there is not the typical hysteresis from corrosion pit growth, such as observed for SSs. For the higher-Cr M327 alloy, there is a lower overall current, despite the slightly greater current in the return sweep as compared to the forward sweep. For the M326 alloy, a higher current was observed; however, the return sweep shows a lower

Neutron Absorber Material Corrosion Testing Report

Identifier:

Revision: 0

Effective Date: 12/17/2020

Page 19 of 52

current than the forward sweep. Overall there is significantly greater current for the M326 alloy. Due to the secondary phase, pitting corrosion of these alloys is more complex. The prevailing (but unproven) thought in past ANA studies has been that corrosion decreases after the secondary phase is dissolved [16].

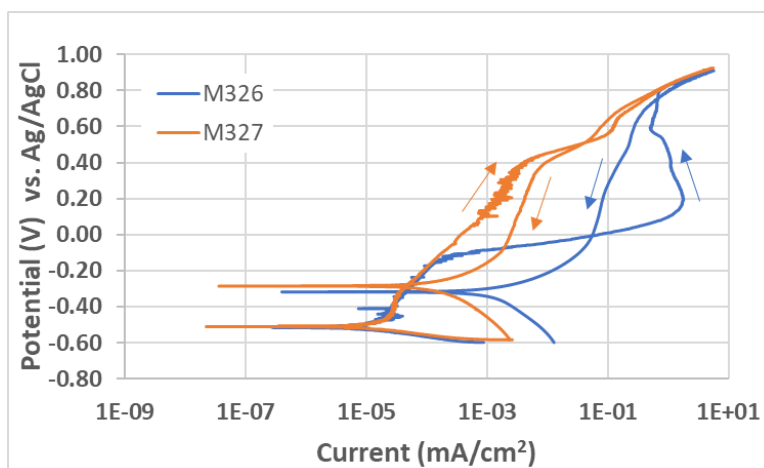


Figure 11. CPP curves for ANA alloys M326 and M327 in seawater.

As the secondary phase impairs the ability to assess ANA stability, tests were performed in which the alloys were pickled in 1 M HCl. Figure 12 shows curves for M326, both before and after 9 days of pickling. There is a significant decrease in the current for the pickled specimen, and the weight loss is significantly lower. This is attributed to the pickling removing the secondary phase. The E_{rp} increases about 0.2 V, as compared to the unpickled specimen.

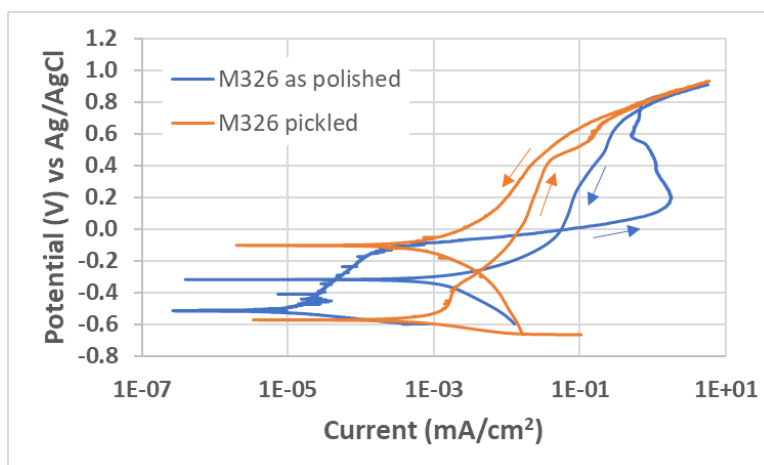


Figure 12. CPP curves for M326 in seawater, as polished and acid-pickled prior to testing.

Neutron Absorber Material Corrosion Testing Report	Identifier:
	Revision: 0
	Effective Date: 12/17/2020

Page 20 of 52

The comparison for M327 is shown in Figure 13. This specimen showed significantly less change in the CPP curve throughout the same duration of pickling. It was noted by lab staff that less hydrogen gas (cathode reaction product of corrosion) was observed for M327 after the first day or so of pickling, whereas the M326 specimen was more continuous with time. There was a slight increase in E_p for the pickled specimen.

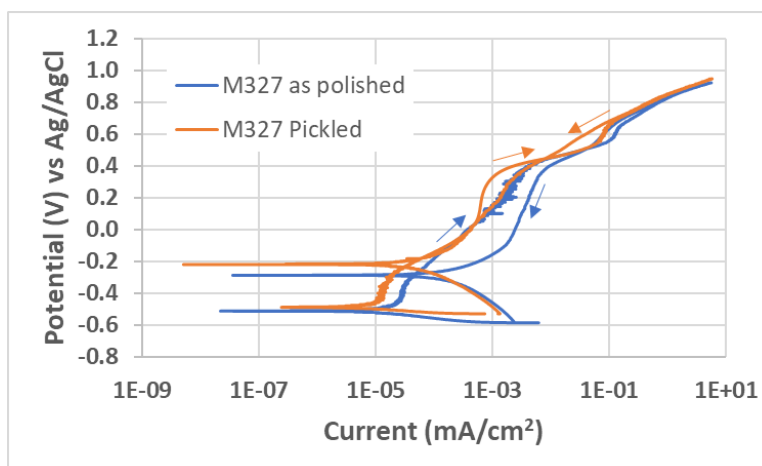


Figure 13. CPP curves for M327 in seawater, as polished and acid-pickled prior to testing.

3.1.3.2 CPP results in 0.028 M NaCl

Results for the benchmark SS alloys in 0.028 M NaCl are shown in Figure 14. These alloys both show an active corrosion feature of between -0.2 and -0.4 V, which is more prominent for 304L. For 304L, the current in the forward sweep increases earlier than that of 316L. On the return sweep, the 316L has a defined E_p crossing zero current; 304L decreases at a somewhat lower potential than 316L, but the current transitions to a second peak at around -0.3 V before crossing zero current. The lack of a crossing is thought to be due to the transition from pitting corrosion to active general corrosion.

Neutron Absorber Material Corrosion Testing Report

Identifier:

Revision: 0

Effective Date: 12/17/2020

Page 21 of 52

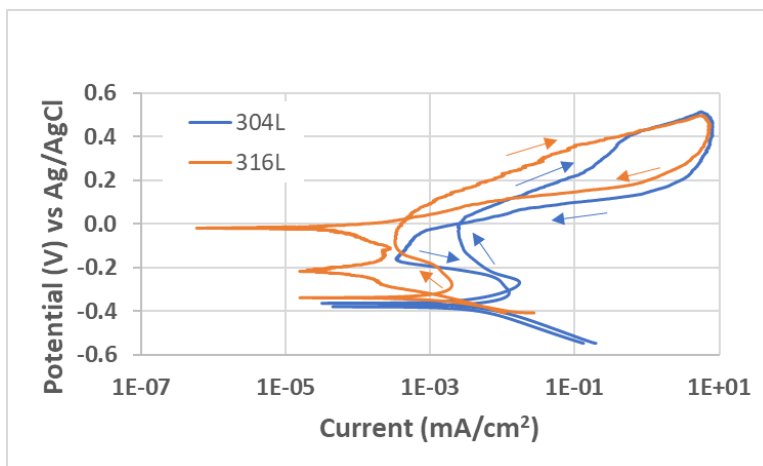


Figure 14. CPP curves for Types 304L and 316L SS in 0.028 M NaCl.

CPP curves for BSS specimens are shown in Figure 15. On the forward sweep, it is noted that the 304B5 specimen has a delayed increase compared to 304B4. Note that this was observed in more dilute solutions in previous testing for specimens cut from the same two plates [17]. The return sweep shows a poorly defined drop in current on the return sweep; 304B4 shows only a slightly more positive potential during repassivation, but plateaus at a higher current than 304B5.

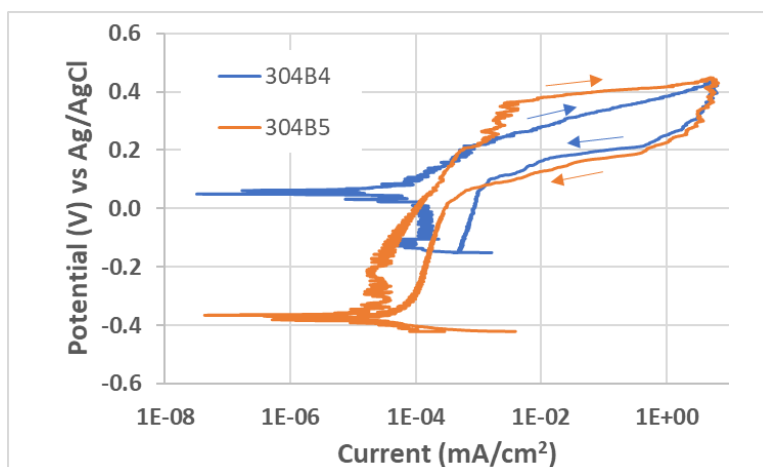


Figure 15. CPP curves for 304B4 and 304B5 alloys in 0.028 M NaCl.

The CPP curve for Alloy 22 is shown in Figure 16. This curve displays behavior expected of a corrosion-resistant material: no sign of pitting and a very positive E_{rp} value at around 0.4 V. It is not clear why noise is observed in the forward sweep; however, the current is lower than that measured for most other alloys, and the solution conductivity is lower.

Neutron Absorber Material Corrosion Testing Report

Identifier:

Revision: 0

Effective Date: 12/17/2020

Page 22 of 52

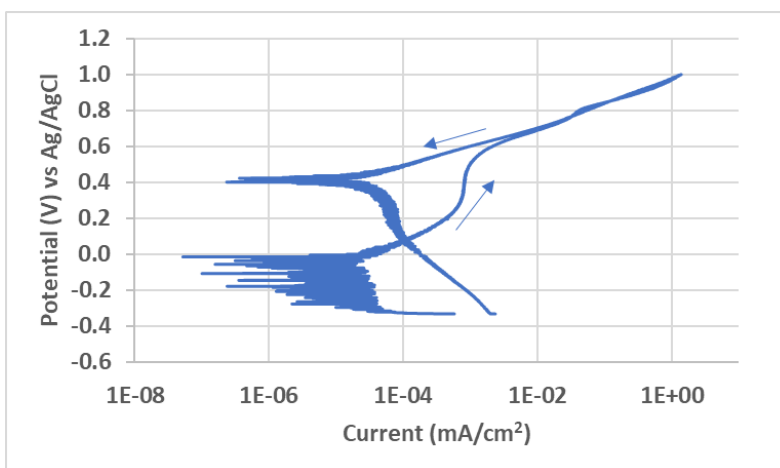


Figure 16. CPP curves for Alloy 22 in 0.028 M NaCl.

CPP curves for ANA specimens in 0.028 M NaCl are shown in Figure 17. As observed in seawater, there is significant current in the forward sweep, attributable to the dissolution of the secondary phase. On the return sweep, the current is decreased, presumably due to dissolution of most of the surface-exposed secondary phase. Both specimens show a very negative E_{rp} of around -0.3 V.

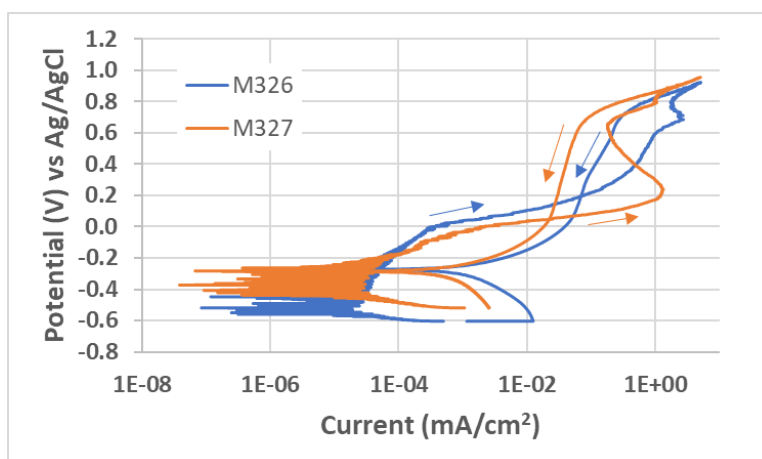


Figure 17. CPP curves for ANA alloys M326 and M327 in 0.028 M NaCl.

3.1.3.3 CPP results in 0.1 M HCl

Curves for the SS alloys in 0.1 M HCl are shown in Figure 18. Both curves show similar features, with a large hysteresis loop at the positive limit. The 316L specimen shows a clear E_{rp} value where the current crosses zero, while the 304L specimen transitions into active corrosion similar to that observed for 0.028 M NaCl. Passive corrosion is more pronounced in the acidic condition and is supported by the higher general corrosion rates observed by LPR in this solution.

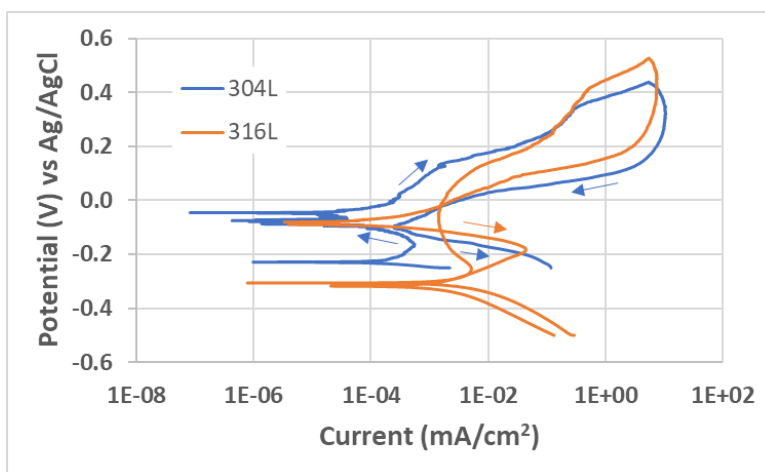


Figure 18. CPP curves for Types 304L and 316L SS in 0.1 M HCl.

Figure 19 shows CPP sweeps for BSS alloys in 0.1 M HCl. Corrosion in the active region is more pronounced than that observed for the SS alloys shown above. The curves are similar in shape, with pitting transitioning directly into a strong peak in the active dissolution region without defined E_{rp} values.

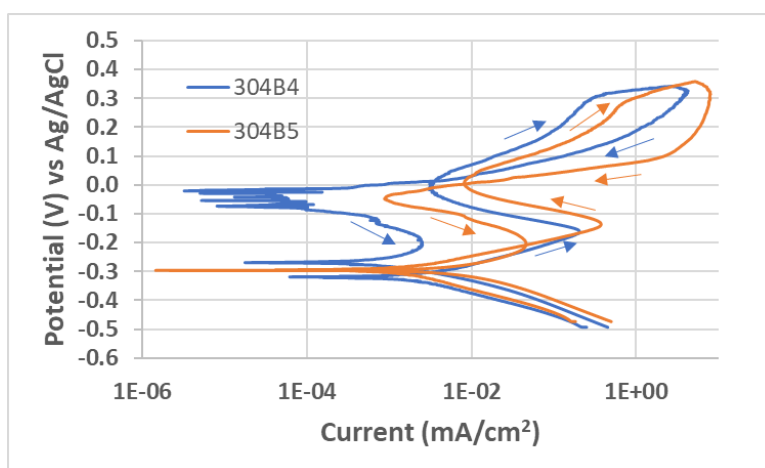


Figure 19. CPP curves for 304B4 and 304B5 alloys in 0.1 M HCl.

Figure 20 shows a CPP curve for Alloy 22 in 0.1 M HCl. The curve demonstrates the high level of corrosion resistance for this alloy in acidic chloride, with no pitting signatures observed and a very positive E_{rp} near 0.7 V.

Neutron Absorber Material Corrosion Testing Report

Identifier:

Revision: 0

Effective Date: 12/17/2020

Page 24 of 52

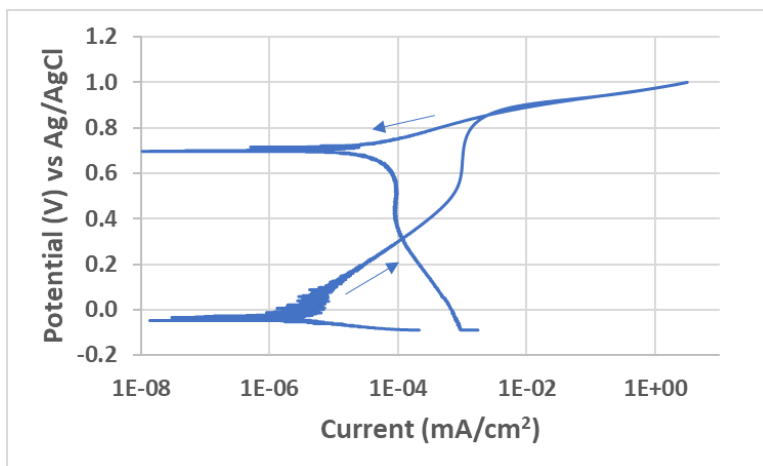


Figure 20. CPP curves for Alloy 22 in 0.1 M HCl.

CPP curves for the ANA specimens in 0.1 M HCl are shown in Figure 21. There is a significant difference between the curves, with higher current being observed for M326. Both curves show a decrease in the current on the return sweep, indicating dissolution of the surface-accessible secondary phase. The M327 (higher-Cr) alloy shows much better passivation, with an E_{rp} of around 0 V. The M326 specimen has significant current extending back to where it transitions to repassivation at around -0.2 V.

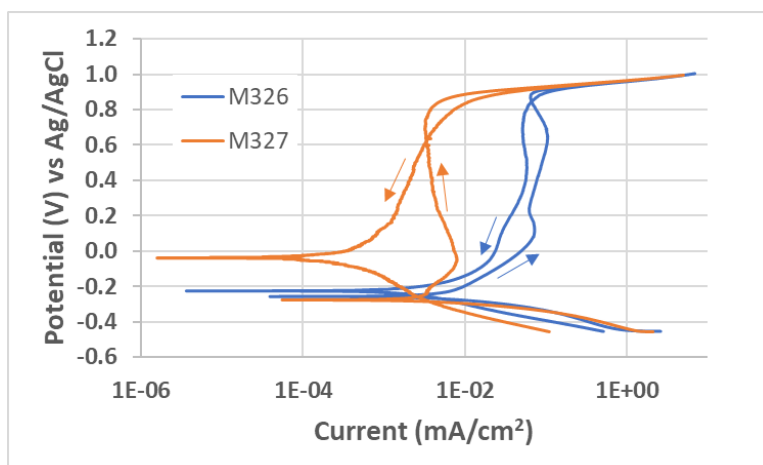


Figure 21. CPP curves for ANA alloys M326 and M327 in 0.1 M HCl.

The ANA specimens pose a challenge to assessment, due to the presence of a reactive secondary phase (Ni_5Gd). ANA specimens were pickled in 1 M HCl for several days to dissolve the secondary phase. Specimens were then put through the test sequence for evaluation as shown in Figure 22. The curve for the pickled specimen shows a much lower current and a positive shift in the E_{rp} . The curve for the pickled

Neutron Absorber Material Corrosion Testing Report	Identifier:
	Revision: 0
	Effective Date: 12/17/2020

Page 25 of 52

specimen is closer to that for Alloy 22 in Figure 20. In potentiostatic testing performed in 0.1 M HCl at 0.2 V vs. saturated calomel electrode, the current values for these two alloys were quite similar [16].

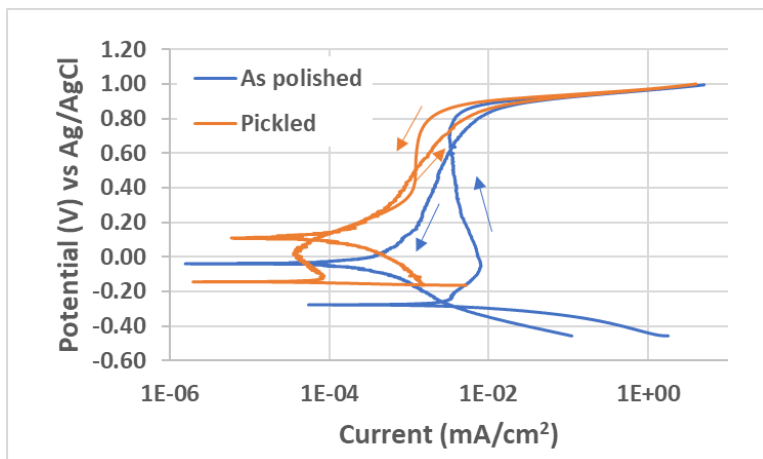


Figure 22. CPP curves for M327 in 0.1 M HCl, as polished and after acid pickling.

3.1.3.4 Parameters from CPP curves

An initial assessment of the CPP curves for all three solutions was performed, as reported in Table 4. In some cases, the CPP curves do not allow for definitive values to be reported. Table 4 includes initial testing data employing lower switching potentials that are valid but do not fully initiate pitting corrosion. Because these tests did not scan as far into pitting (with a lower overall charge), they have lower pitting damage and lower weight loss, as reported in Section 3.1.4.1 below.

Nickel alloys generally do not show signs of localized corrosion in the CPP curves. The fact that Alloy 22 did not show signs of pitting corrosion agrees with previous work [4]. The reported E_{rp} values for Alloy 22 are far positive of the other alloys. However, since pitting corrosion is not observed, a true E_{rp} cannot be determined for Alloy 22 in these environments (more aggressive environments are needed). ANA specimens show unique CPP curves, as detailed above. Based on previous work [16], surface damage to the specimens appears limited to locations where secondary phase particles intersect the surface. Characteristics of the curves are based on the level to which the secondary phase has been dissolved. As an example, for M327 in 0.1 M HCl, the curve on 8/21/2020 scanned more positive (before the switching potential) than the one for 08/10/2020 and showed a more positive E_{rp} . Presumably, the more positive scan in the most corrosive solution removed more of the secondary phase intersecting the surface. A more positive E_{rp} indicates a more corrosion-resistant material. To further demonstrate this, a specimen was pickled (as described previously), and a positive shift was observed in the E_{rp} , (11/05/2020 in 0.1 M HCl), suggesting that the secondary phase shifts E_{rp} negative. Similar trends were observed for specimens in

Idaho National Laboratory

Neutron Absorber Material Corrosion
Testing Report

Identifier:

Revision: 0

Effective Date: 12/17/2020

Page 26 of 52

seawater; however, it appears the specimens were insufficiently treated (9 days vs. 29 days). A systematic pickling study is underway and will be reported on sometime in the future.

In all cases, SS specimens showed signs of pitting corrosion in CPP sweeps with large hysteresis loops. As discussed above, SS specimens seldom showed a defined E_{rp} value, as the current seldom crossed zero. This is thought to be due to the overlap between pit repassivation and active corrosion regions. The values presented in Table 4 were selected as the point where current plateaus following the rapid decrease from pitting corrosion. In future work, advice on how to treat this situation will be sought in the literature and standards. In the current assessment, E_{rp} was not significantly different for the SS alloys. However, the E_{pit} for 316L in seawater was significantly more positive than for the other SS alloys, suggesting a lower probability of initiating corrosion. It is interesting that the 304B5 and 316L specimens showed fewer transients (were smoother) in E_{corr} traces as compared to 304B4 and 304L—likely correlating to increased E_{pit} values. This certainly could influence in-service pitting damage in a probabilistic way.

Table 4. Corrosion parameters obtained from CPP tests.

Date	Alloy	Solution	E_{corr}	E_{rp}	E_{pit}	Hysteresis loop	E_{corr}	Sweep range
7/27/2020*	Alloy 22	0.028 M NaCl	-0.0026	0.366	none	N	S	L
10/30/2020	Alloy 22	0.028 M NaCl	-0.0464	0.401	none	N	S	F
8/6/2020*	M327	0.028 M NaCl	-0.0534	-0.343	-0.164	S	T	L
8/19/2020	M327	0.028 M NaCl	-0.135	-0.285	none	N	T	F
8/11/2020*	M326	0.028 M NaCl	-0.0891	-0.335	-0.0349	S	T	L
8/17/2020*	M326	0.028 M NaCl	-0.137	-0.324	none	N	T	L
8/21/2020	M326	0.028 M NaCl	-0.141	-0.273	none	N	T	F
7/29/2020*	316L	0.028 M NaCl	0.0237	0.0828	0.339	L	S	L
10/28/2020	316L	0.028 M NaCl	0.0544	-0.0197	0.352	L	T	F
8/3/2020*	304L	0.028 M NaCl	0.0223	-0.0938	0.267	L	T	L
10/27/2020	304L	0.028 M NaCl	-	-0.0293	0.372	L	T	F
8/26/2020	304B4	0.028 M NaCl	0.0163	0.0645	0.345	L	T	L
9/4/2020	304B4	0.028 M NaCl	0.0606	0.0544	0.216	L	T	F
9/8/2020	304B5	0.028 M NaCl	-0.0384	0.0189	0.365	L	T	F
7/28/2020*	Alloy 22	Seawater	-0.144	0.19	none	N	S	L
9/22/2020	Alloy 22	Seawater	-0.111	0.236	none	N	S	F
8/7/2020*	M327	Seawater	-0.127	-0.353	-0.0676	S	T	L
8/26/2020	M327	Seawater	-0.291	-0.285	0.448	S	T	F
11/12/2020	M327P	Seawater	-0.207	-0.218	none	N	S	F
8/12/2020*	M326	Seawater	-0.174	-0.388	-0.153	S	T	L
8/20/2020	M326	Seawater	-0.189	-0.317	none	N	T	F

Idaho National Laboratory

Neutron Absorber Material Corrosion
Testing Report

Identifier:

Revision: 0

Effective Date: 12/17/2020

Page 27 of 52

11/13/2020	M326P	Seawater	-0.327	-0.103	none	N	S	F
7/30/2020*	316L	Seawater	-0.0837	-0.075	0.362	L	S	L
9/2/2020	316L	Seawater	-0.0479	-0.0756	0.348	L	S	F
8/4/2020*	304L	Seawater	-0.033	-0.137	0.156	L	T	L
9/15/2020	304L	Seawater	-0.0205	-0.0754	0.107	L	T	F
9/1/2020	304B4	Seawater	-0.0142	-0.0236	0.207	L	T	F
9/3/2020	304B4	Seawater	-0.0502	-0.0249	0.133	L	T	F
9/9/2020	304B5	Seawater	-0.0998	-0.0862	0.214	L	T	F
7/29/2020*	Alloy 22	0.1 M HCl	0.141	0.51	none	N	S	L
11/9/2020	Alloy 22	0.1 M HCl	0.145	0.697	none	N	T	F
8/10/2020*	M327	0.1 M HCl	-0.273	-0.217	none	N	-	L
8/21/2020	M327	0.1 M HCl	-0.226	-0.0392	none	N	S	F
11/5/2020	M327P	0.1 M HCl	0.0867	0.110	none	N	T	F
8/18/2020	M326	0.1 M HCl	-0.216	-0.244	none	N	S	L
8/27/2020	M326	0.1 M HCl	-0.227	-0.226	none	S	T	F
7/30/2020*	316L	0.1 M HCl	-0.0179	-0.199	0.109	S	T	L
11/5/2020	316L	0.1 M HCl	-0.0147	-0.0806	0.245	L	T	F
8/5/2020*	304L	0.1 M HCl	-0.0191	-0.0642	0.116	L	T	L
11/5/2020	304L	0.1 M HCl	-0.0392	-0.0968	0.138	L	T	F
8/27/2020	304B4	0.1 M HCl	-0.239	-0.0207	0.307	L	T	L
9/10/2020	304B5	0.1 M HCl	-0.239	-0.3	0.0441	S	T	F

Hysteresis loop: none (N), small (S), large (L),

E_{corr}: smooth (S), transients (T)

** Tests in which the switching potential was lower*

Summary for 0.028 M NaCl: This solution showed CPP curves for SS specimens that had classic pit initiation and hysteresis loops on the return sweep. There does not appear to be a significant difference in the SS curves. There was also the presence of an active corrosion feature for 304L and 316L; it was not present for the borated SS, possibly due to higher Cr content. The ANA specimens show large current in the passive region due to dissolution of the secondary phase. However, this current tended to decrease on the return sweep, suggesting this was not a typical pitting feature, such as is associated with SS materials. The mechanism does not appear to be pit initiation and growth but more of a selective dissolution of the reactive secondary phase. Alloy 22 showed no sign of pitting corrosion and very low current in the active and passive range. The current at the positive limit is ascribed to transpassive dissolution of Cr.

Summary for seawater: Results are very similar to what was observed for 0.028 M NaCl, except that active corrosion is not observed for any SS alloys in seawater. It is unclear if the presence of sulfate passivates specimens to active corrosion, and additional review of the literature is needed. ANA specimens and Alloy 22 show similar behavior as well.

Idaho National Laboratory

Neutron Absorber Material Corrosion Testing Report	Identifier:
	Revision: 0
	Effective Date: 12/17/2020

Identifier:		
Revision: 0		
Effective Date: 12/17/2020		Page 28 of 52

Summary for 0.1 M HCl: As expected, this solution was very aggressive to SS specimens, with all SS alloys showing significant current in the active region and generally more negative E_{rp} values. The ANA specimens do not seem to be impacted strongly, but the higher-Cr M327 shows significantly lower current in the active and passive regions (Figure 21). Given that both alloys have similar Gd levels (and thus similar secondary phase volumes), the greater current for M326 suggests that some primary phase is dissolving and will be the focus of investigations in the future. The results are pointing to selecting the higher Cr ANA alloy.

3.1.4 Post-test observations

3.1.4.1 Gravimetric results and observations

Specimens were weighed and photographed before and after testing. Table 5 presents the weight change scaled to surface area and provides visual observations captured by photographs. For localized corrosion, which appears to be the prime weight loss mechanism, the weight change should not be considered proportional to the corrosion rate. Note that the reversing potential for the forward sweep greatly influences the weight loss. In some cases, the measurement can be used to assess test results. Given the quite different CPP curves, standardizing the reversing potential does not make sense. Of particular note are the pickled ANA specimens: M327 pickled for a longer time showed almost no weight loss (tested in 0.1 M HCl), while ANA specimens pickled for a shorter time still showed weight loss (tested in seawater). This suggests that the pickling was insufficient in the latter case (Observations are based on notebook records and photographs taken after testing).

Table 5. Gravimetric analysis and observations made after CPP tests.

Date	Alloy	Solution	Wt change (g/cm ²)	Visual observations
7/27/2020*	Alloy 22	0.028 M NaCl	0.00000	No clear change
10/30/2020	Alloy 22	0.028M NaCl	-0.00016	Faint brown finish, no pits observed
8/6/2020*	M327	0.028 M NaCl	-0.00001	No clear change
8/19/2020	M327	0.028 M NaCl	-0.00163	Dull with localized stains, widespread shallow pits
8/11/2020*	M326	0.028 M NaCl	-0.00198	Mostly shiny, brown stains, shallow pits
8/17/2020*	M326	0.028 M NaCl	-0.00150	Bright, widespread shallow pits
8/21/2020	M326	0.028 M NaCl	-0.00221	Dull, widespread shallow pits
7/29/2020*	316L	0.028 M NaCl	0.00000	No clear change
10/28/2020	316L	0.028 M NaCl	-0.00335	Dull brown iridescent finish, widespread pitting
8/3/2020*	304L	0.028M NaCl	-0.00001	No clear change
10/27/2020	304L	0.028 M NaCl	-0.00261	Dull gray/brown streaks, no clear pits

Idaho National Laboratory

Neutron Absorber Material Corrosion
Testing Report

Identifier:

Revision: 0

Effective Date: 12/17/2020

Page 29 of 52

8/26/2020	304B4	0.028 M NaCl	-0.00111	Shiny with localized brown stains, hint of pits
9/4/2020	304B4	0.028 M NaCl	-0.00143	Shiny, widespread small pits
9/8/2020	304B5	0.028 M NaCl	-0.00153	Shiny, widespread small pits
7/28/2020*	Alloy 22	Seawater	-0.00055	No clear change
9/22/2020	Alloy 22	Seawater	-0.00042	Dull brown, no clear pits observed
8/7/2020*	M327	Seawater	0.00001	Widespread shallow pits
8/26/2020	M327	Seawater	-0.00060	Dull, widespread shallow pits
11/12/2020	M327P	Seawater	-0.00071	Iridescent finish, very small pits
8/12/2020*	M326	Seawater	-0.00236	Mostly shiny, isolated brown stains, shallow pits
8/20/2020	M326	Seawater	-0.00235	Dull, shallow widespread pits
11/13/2020	M326P	Seawater	-0.00086	Dull iridescent finish w/ scattered pitting
7/30/2020*	316L	Seawater	0.00032	Brown coloration, no pitting
9/2/2020	316L	Seawater	-0.01136	Dull with widespread, long narrow pits
8/4/2020*	304L	Seawater	0.00000	Mostly shiny, no pitting
9/15/2020	304L	Seawater	-0.01071	Shiny with brown stains, narrow deep pits
9/3/2020	304B4	Seawater	-0.00317	Dull, widespread pitting
9/9/2020	304B5	Seawater	-0.00769	Dull, widespread, deep but small pits
7/29/2020*	Alloy 22	0.1 M HCl	0.00000	No clear change
11/9/2020	Alloy 22	0.1M HCl	-0.00016	Very faint dull brown finish, no pitting observed
8/10/2020*	M327	0.1M HCl	-0.00072	No clear change
8/21/2020	M327	0.1M HCl	-0.00029	Mostly shiny, local brown stains, shallow pits
11/5/2020	M327P	0.1M HCl	-0.00004	Faint dull finish, widespread pits
8/13/2020*	M326	0.1M HCl	-0.00142	Dull from brown stains widespread pits
8/27/2020	M326	0.1M HCl	-0.00091	Rainbow coloration, widespread shallow pits
7/30/2020*	316L	0.1 M HCl	-0.00004	No clear change
11/5/2020	316L	0.1M HCl	-0.00391	Shiny with pitting across specimen
8/5/2020*	304L	0.1 M HCl	-0.00194	Mostly shiny, long, shallow pits
11/5/2020	304L	0.1M HCl	-0.00462	Shiny with pitting across specimen
8/27/2020	304B4	0.1M HCl	-0.00153	Dull, widespread deep pits
9/10/2020	304B5	0.1M HCl	-0.00336	Dull, widespread localized small pits

* Tests in which the switching potential was lower

3.1.4.2 Post-test images

Figures 23–25 show specimen photographs taken after testing in seawater, 0.028 M NaCl, and 0.1 M HCl, respectively. The cylindrical specimen geometry does not lend itself to photography, but, in general, the images provide additional qualitative information on the damage incurred during testing. Note that tests were not all performed to similar levels, as nickel alloys were scanned much more positive than the SS and BSS specimens. Specimens tested in seawater show staining, particularly for SS specimens. SS and BSS specimens show pits distributed across their surfaces. Alloy 22 shows limited changes in its surface,

**Neutron Absorber Material Corrosion
Testing Report**

Identifier:

Revision: 0

Effective Date: 12/17/2020

Page 30 of 52

except for some light tan coloration after being in seawater. The ANA specimens have shallow pits evenly distributed across their entire surfaces. SS and BSS specimens tested in seawater show extensive rust deposits that appear to have originated from pitting sites. Note that the M326 specimen showed extensive staining in 0.1 M HCl, although an incommensurate amount of surface damage was observed. The coloration of the stain is likely due to variation in oxide film thickness, probably resulting from deposition of the dissolved secondary phase and perhaps some primary phase material as well.

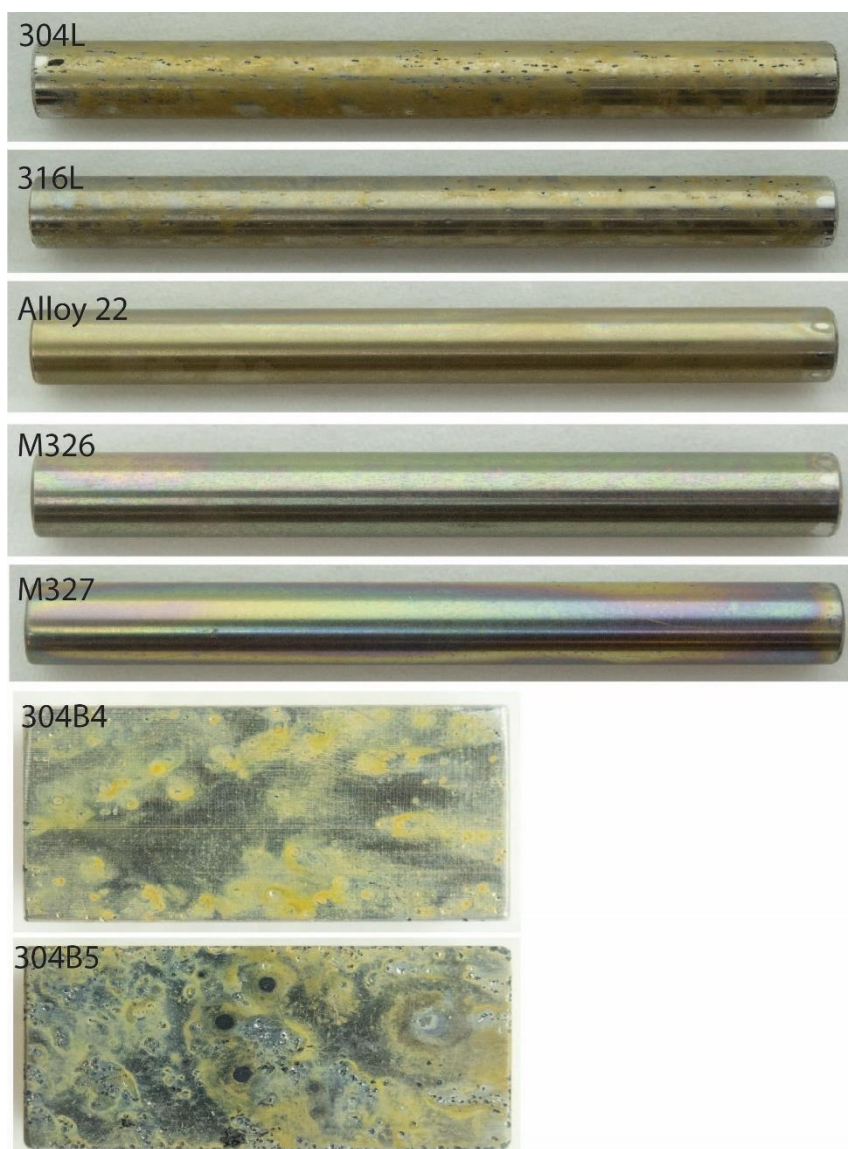


Figure 23. Images of specimens tested in seawater.

**Neutron Absorber Material Corrosion
Testing Report**

Identifier:

Revision: 0

Effective Date: 12/17/2020

Page 31 of 52

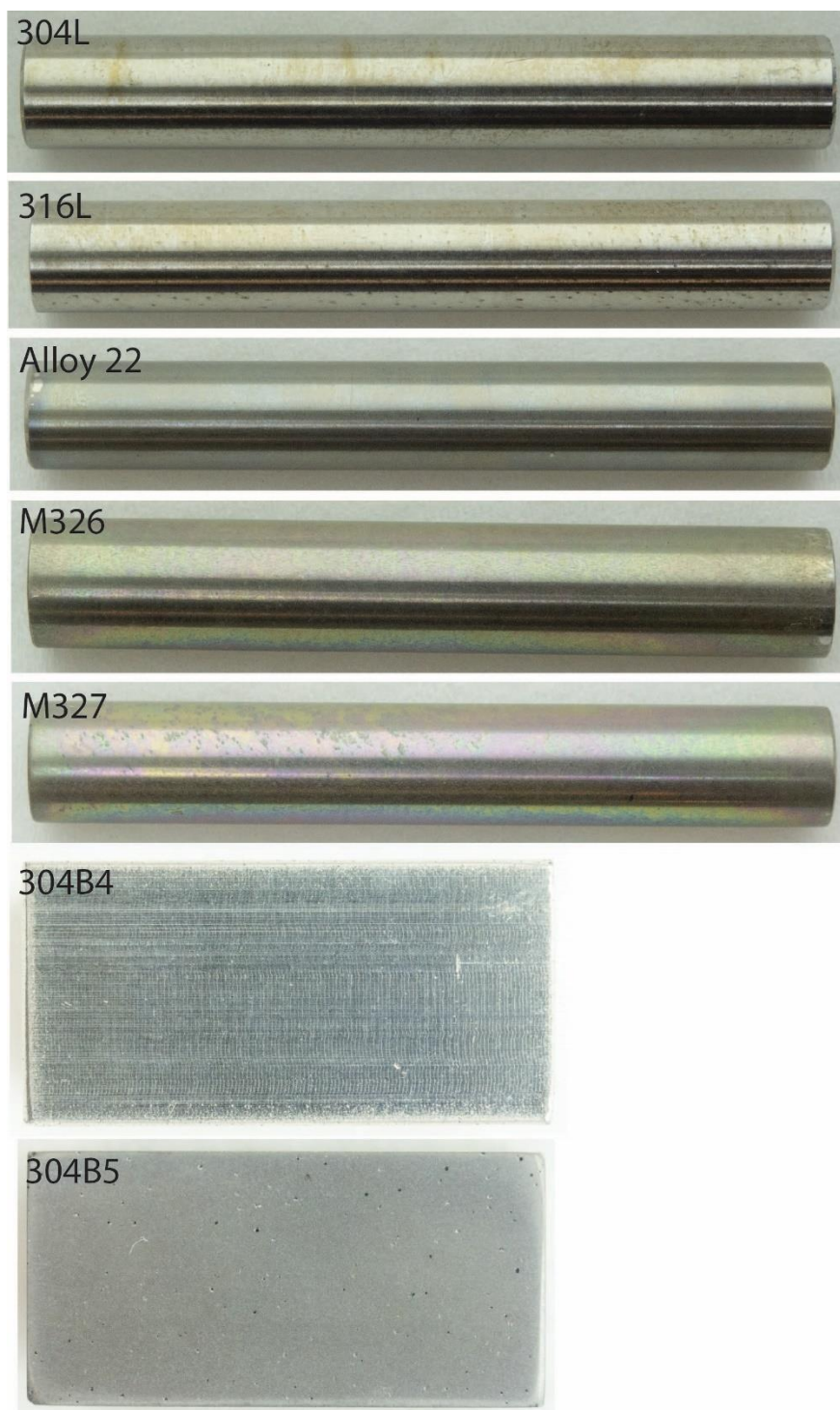


Figure 24. Images of specimens tested in 0.028 M NaCl.

**Neutron Absorber Material Corrosion
Testing Report**

Identifier:

Revision: 0

Effective Date: 12/17/2020

Page 32 of 52

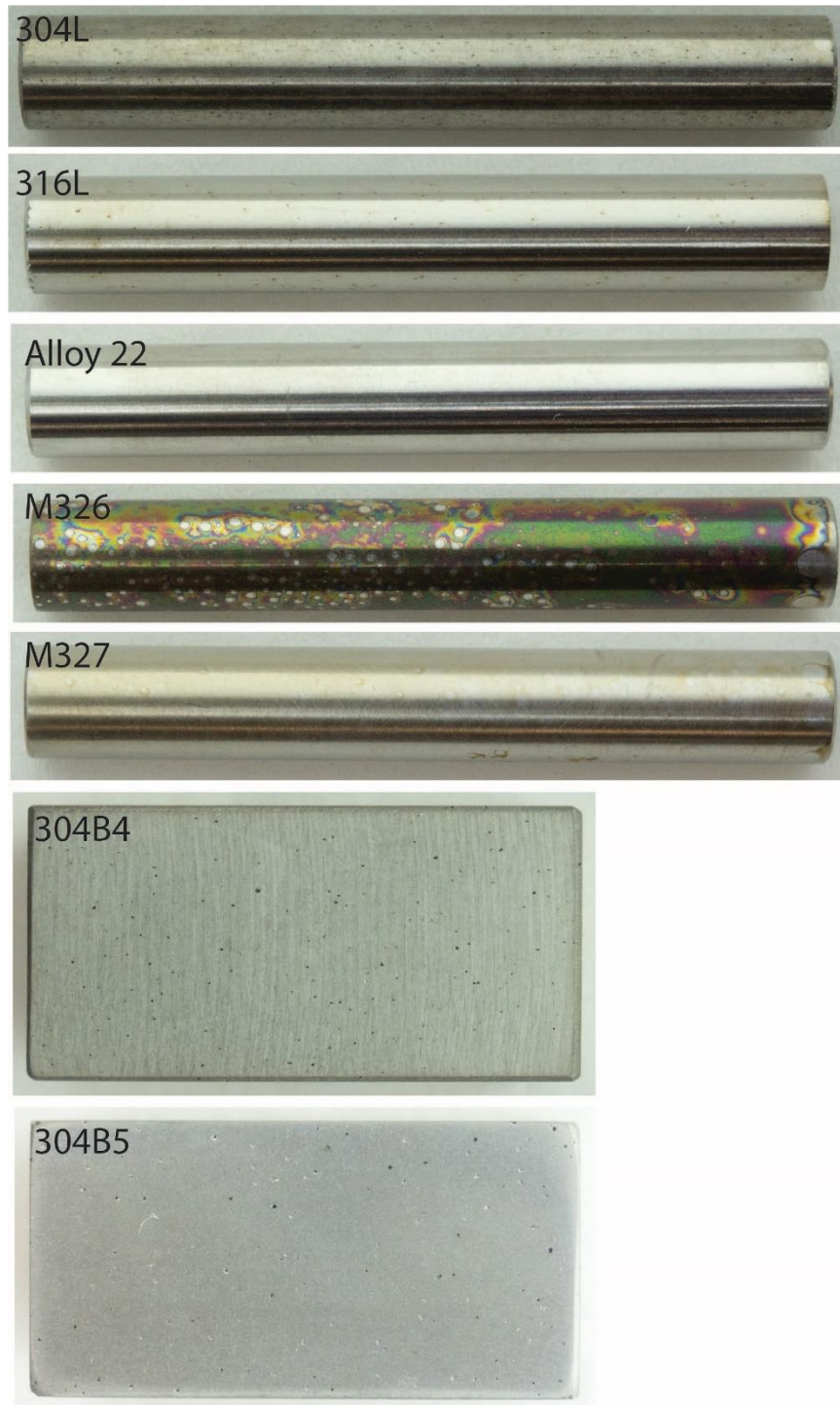


Figure 25. Images of specimens tested in 0.1 M HCl.

**Neutron Absorber Material Corrosion
Testing Report**

Identifier:

Revision: 0

Effective Date: 12/17/2020

Page 33 of 52

3.1.4.3 Post-test SEM images

Figures 26–28 show SEM images of specimens after testing in seawater. All specimens show signs of localized pitting corrosion except for Alloy 22, in which damage appears to be due to mechanical polishing defects. The SS and BSS specimens show a smaller number of well-developed pits. The sizes of these pits are hard to estimate, as small openings conceal the extent of damage, where perhaps a thin oxide film is hiding a much larger open space (cavern-like internal damage). See Section 3.1.4.4 for pit depth analysis. Alloy 22 does not show any significant damage, as would be expected from the CPP curves. ANA specimens show numerous shallow pits, arranged in a fashion that suggests secondary-phase dissolution. Unlike the pits in SS, these pits are very open allowing images of the pit bottoms to be captured. Figure 28E shows what appear to be partially dissolved gadolinide particles.

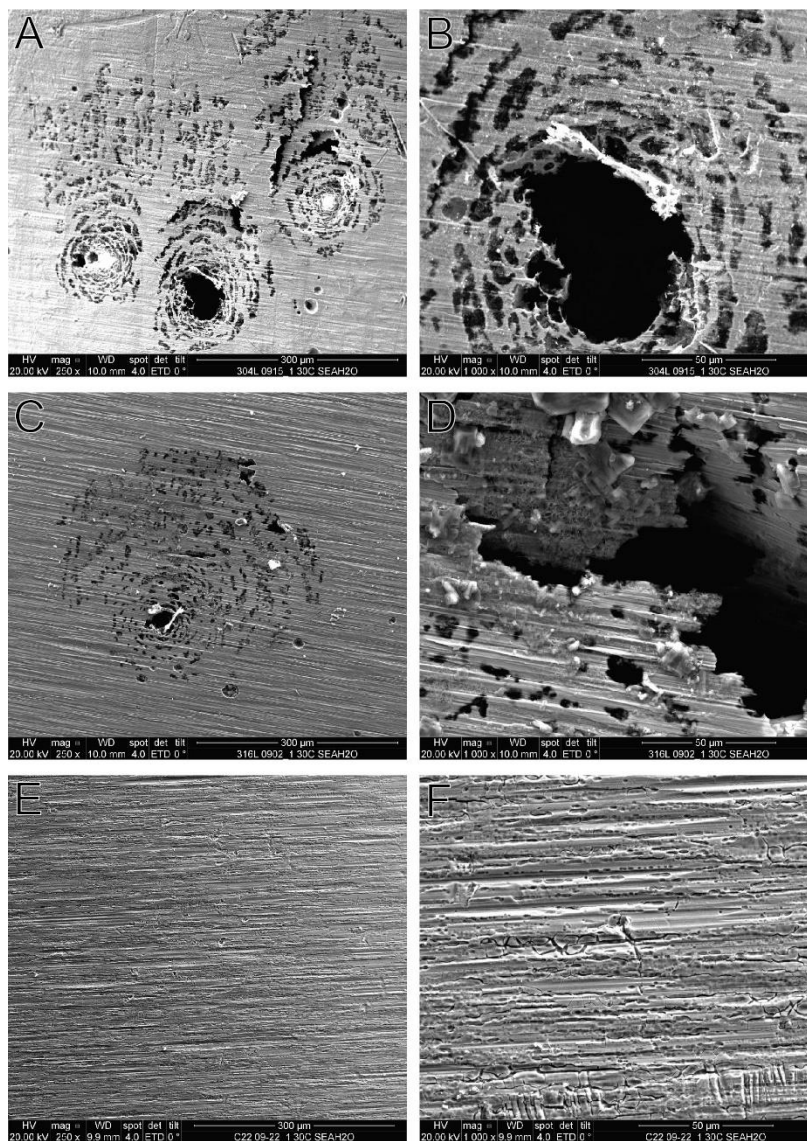


Figure 26. SEM images after testing in seawater at 250x (left) and 1000x (right): A–B) 304L, C–D) 316L, and E–F) Alloy 22.

**Neutron Absorber Material Corrosion
Testing Report**

Identifier:

Revision: 0

Effective Date: 12/17/2020

Page 35 of 52

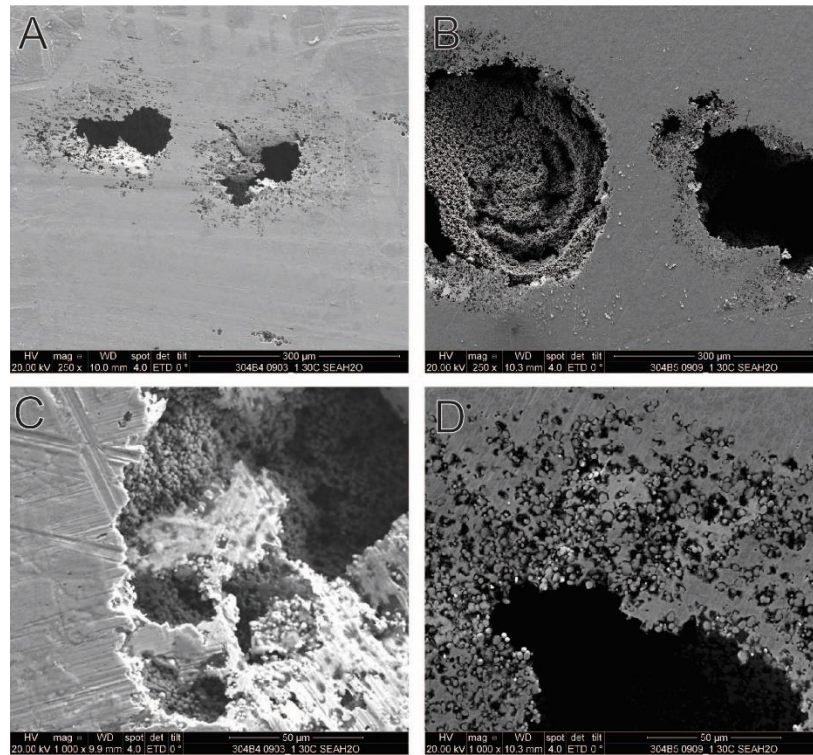


Figure 27. SEM images after testing in seawater at 250x (left) and 1000x (right): A–B) 304B4 and C–D) 304B5.

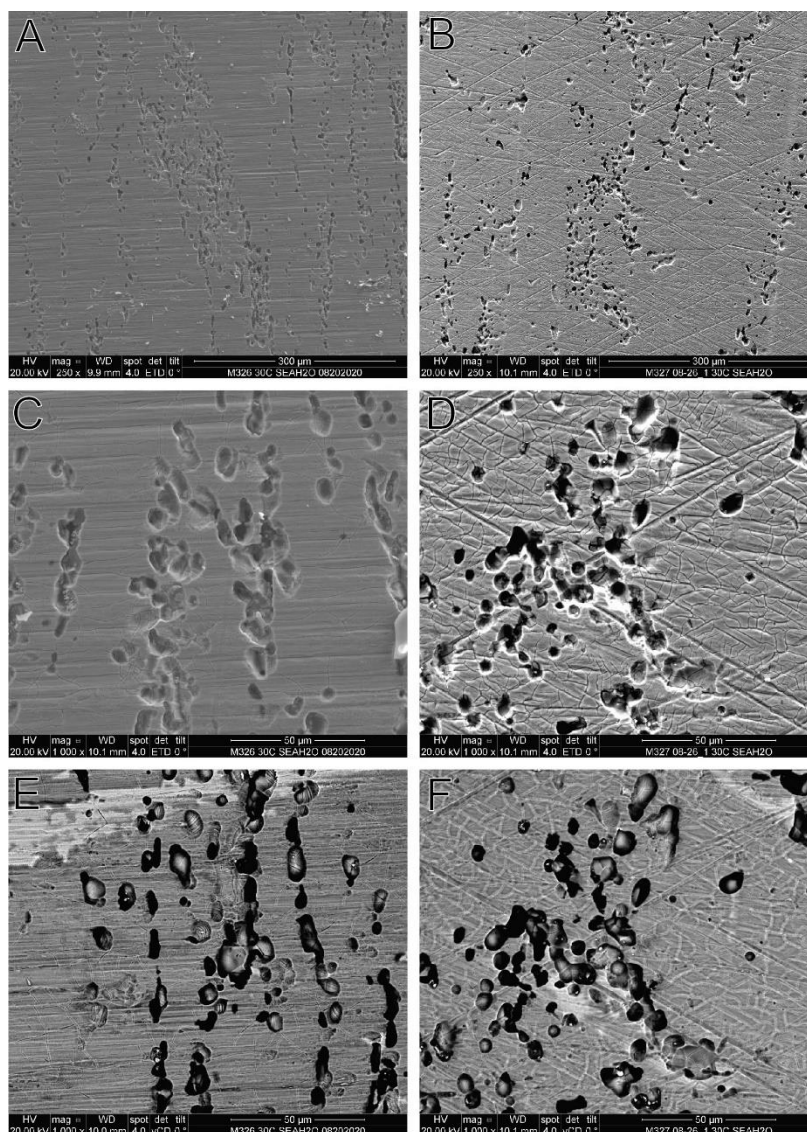


Figure 28. SEM images after testing in seawater for M326 (left) and M327 (right) at 250x (top) and 1000x (middle), and 1000x in backscatter mode (bottom).

Figures 29–31 show SEM images of specimens after testing in 0.028 M NaCl. All the observations from seawater tests largely apply to specimens tested in this environment. Figure 31E shows what appear to be partially dissolved gadolinide (Ni_5Gd) secondary phase particles.

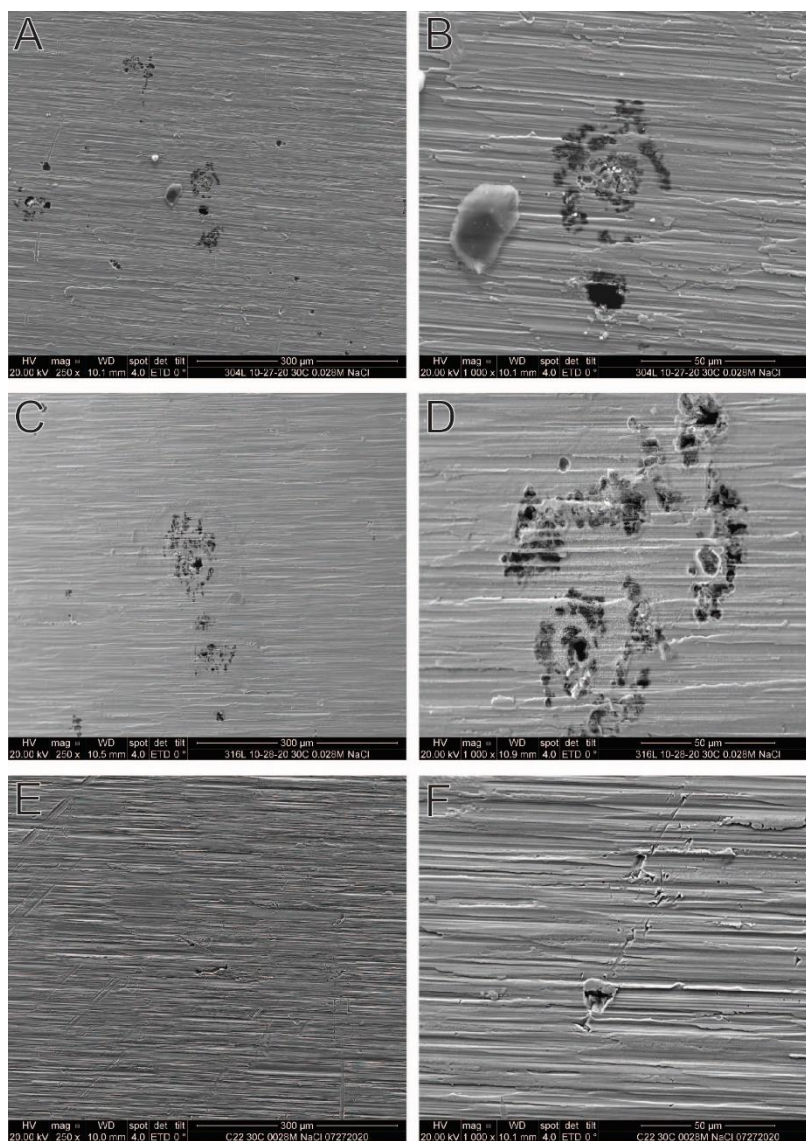


Figure 29. SEM images after testing in 0.028 M NaCl at 250x (left) and 1000x (right): A–B) 304L, C–D) 316L, and E–F) Alloy 22.

**Neutron Absorber Material Corrosion
Testing Report**

Identifier:

Revision: 0

Effective Date: 12/17/2020

Page 38 of 52

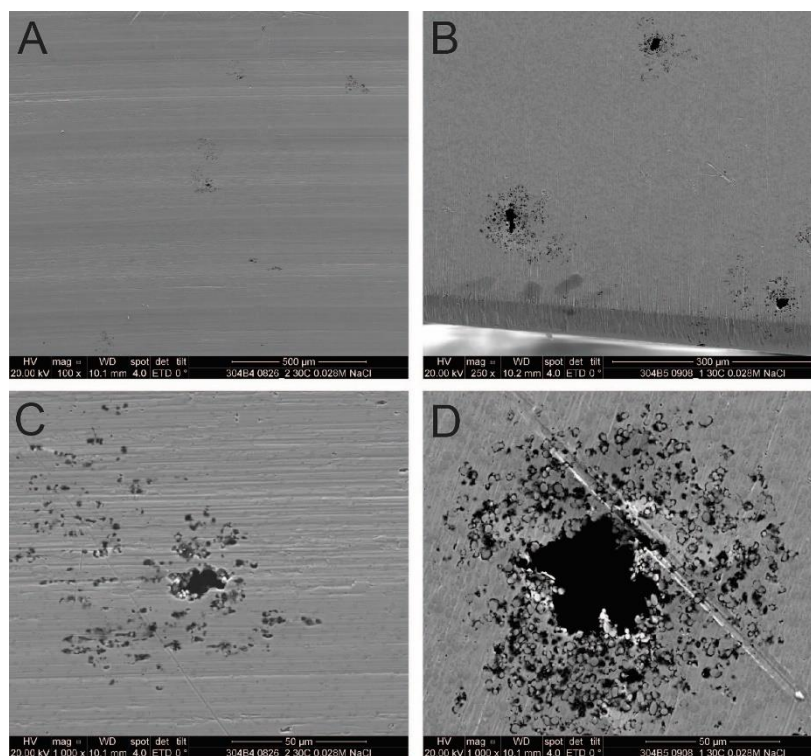


Figure 30. SEM images after testing in 0.028 M NaCl at 250x (left) and 1000x (right): A–B) 304B4 and C–D) 304B5.

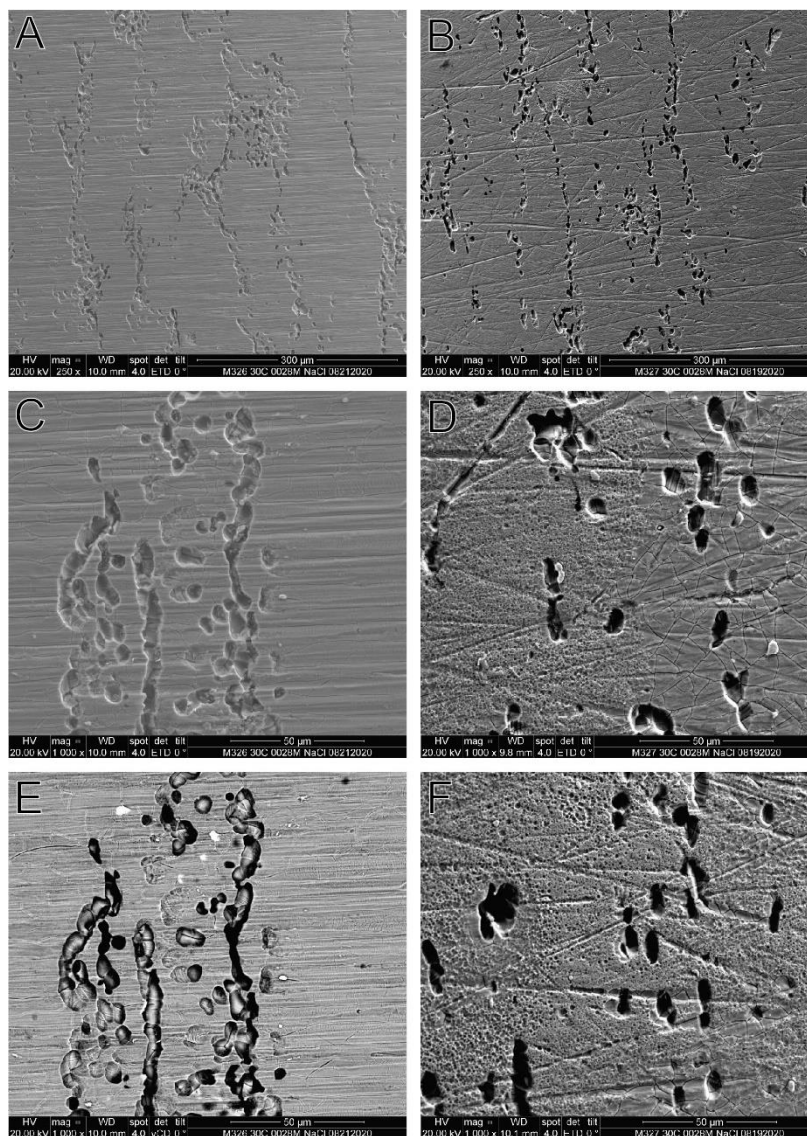


Figure 31. SEM images after testing in 0.028 M NaCl for M326 (left) and M327 (right) at 250x (top) and 1000x (middle), and 1000x in backscatter mode (bottom).

Figures 32–34 show SEM images of specimens after testing in 0.1 M HCl. The pitting is very similar to that measured in the other solutions; however, there are examples of etching in Figures 32B and 33B–D. The ANA specimen shows no discernable change in pit microstructure. Evidence of partially dissolved ANA particles are not observed in this case, likely due to the increased reactivity of the secondary phase at low pH.

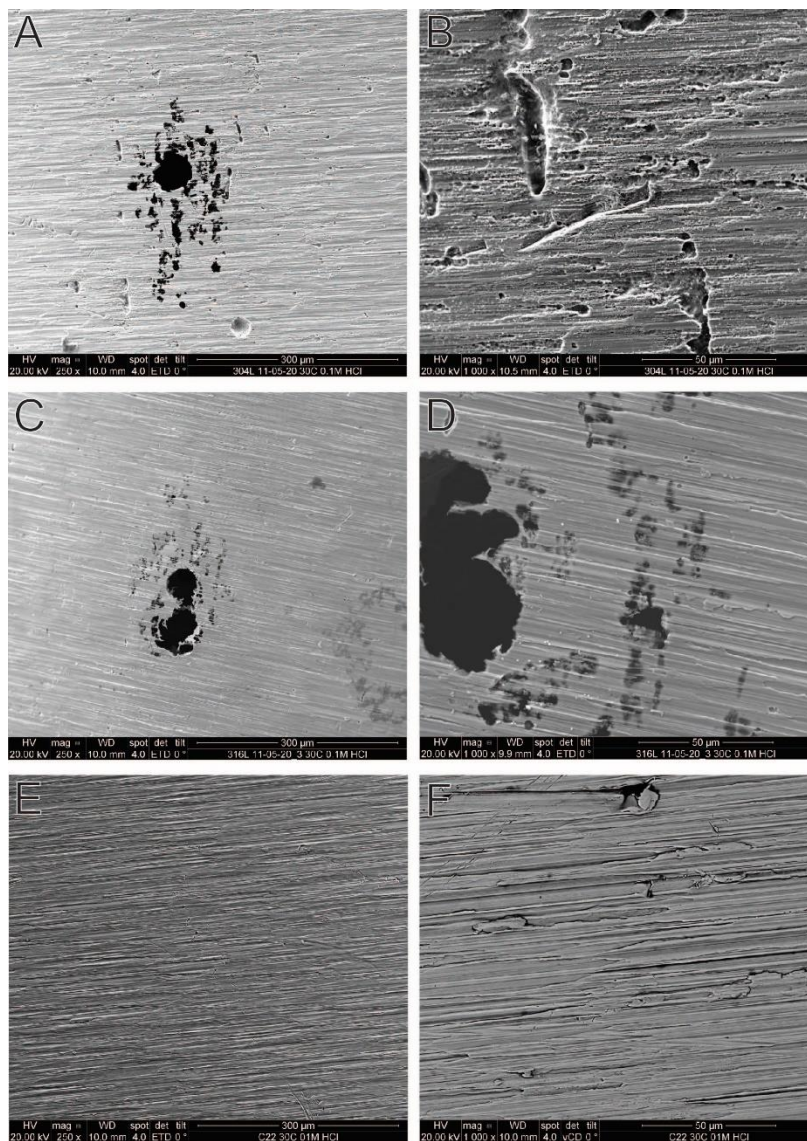


Figure 32. SEM images after testing in 0.1 M HCl at 250x (left) and 1000x (right): A–B) 304L, C–D) 316L, and E–F) Alloy 22.

**Neutron Absorber Material Corrosion
Testing Report**

Identifier:

Revision: 0

Effective Date: 12/17/2020

Page 41 of 52

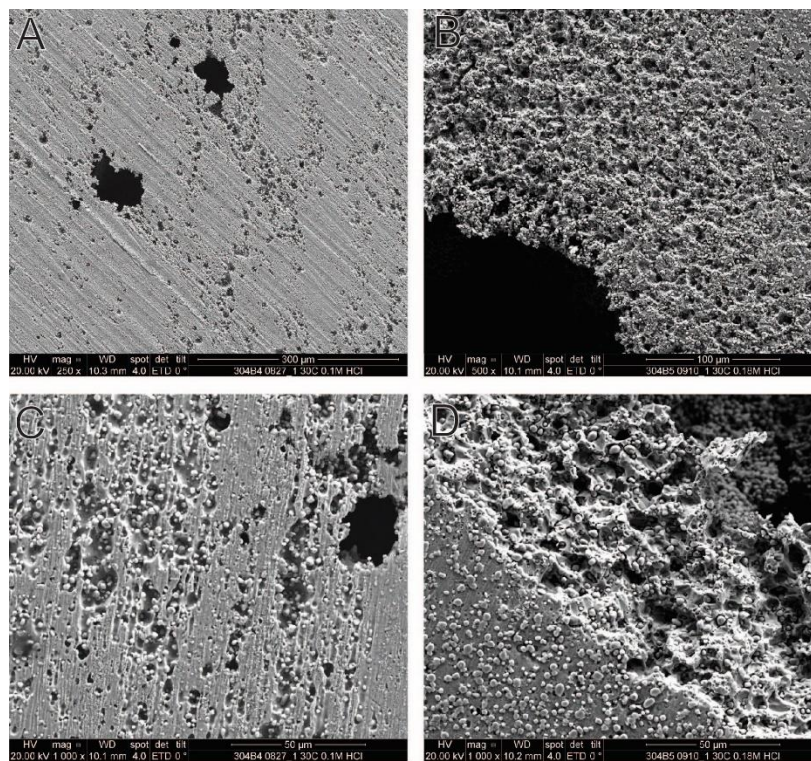


Figure 33. SEM images after testing in 0.1 M HCl at 250x (left) and 1000x (right): A–B) 304B4 and C–D) 304B5.

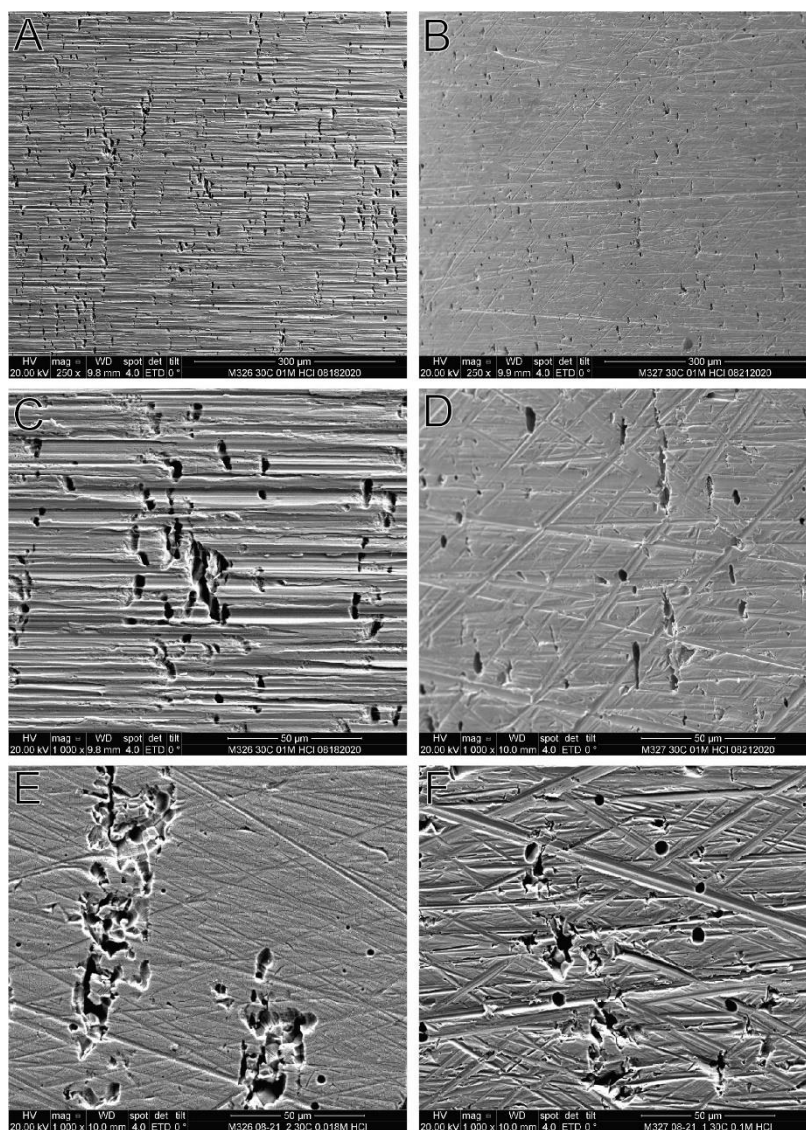


Figure 34. SEM images after testing in 0.1 M HCl for M326 (left) and M327 (right) at 250x (top) and 1000x (middle), and 1000x in backscatter mode (bottom).

3.1.4.4 Pit depth measurements

Pit depths for tested specimens were examined using an optical microscope with calibrated z-range. A summary of this analysis is presented in Table 6. Pit depths are obtained by focusing on the outer surface of the pit, zeroing the depth gauge, then focusing on the pit bottom. These measurements should be used to provide a general idea of the magnitude of pit damage. Note that in many cases—particularly for SS specimens—narrow openings and apparently deep damage prevented observation of the pit bottom. Also note that different switching potentials were used, with the ANA specimens being subjected to more

Idaho National Laboratory

Neutron Absorber Material Corrosion
Testing Report

Identifier:

Revision: 0

Effective Date: 12/17/2020

Page 43 of 52

positive potentials. Despite this, the pit depths are greater for SS specimens. Pits were deepest for seawater and 0.1 M HCl and somewhat shallower for 0.028 M NaCl. The pit depths were all very similar for ANA in all environments, defined by the dissolution of the secondary phase. Note that the standard deviation was very high for SS specimens while being much lower for ANA. This is attributed to the ANA dissolution being primarily confined to the dissolving secondary phase, while the SS corrosion displayed a mixture of shallow and very deep pits and in general not being similarly confined.

Table 6. Average pit depths and brief description.

Date	Alloy	Solution	Avg depth (μm)	Depth SD (μm)	Observations
8/21/2020	M326	0.028M NaCl	4	1.2	Vertical strings of small shallow pits
8/19/2020	M327	0.028M NaCl	3.9	1.9	Vertical strings of small shallow pits
10/27/2020	304L	0.028M NaCl	27.6	60.7	Cavernous pits, strings of shallow pits
10/28/2020	316L	0.028M NaCl	6.9	4	Cavernous pits and strings of shallow pits
9/4/2020	M304B4	0.028 M NaCl	16	18.5	Scattered deep, cavernous pits
9/8/2020	M304B5	0.028 M NaCl	19.1	25.6	Deep pits often encircled by smaller pits
8/20/2020	M326	Seawater	3.1	1.5	Strings of shallow pits
11/3/2020	M326P	Seawater	3	1.2	Strings of shallow pits
8/26/2020	M327	Seawater	3.4	1.4	Strings of shallow pits
11/3/2020	M327P	Seawater	3.8	1.2	Stringed shallow pits
9/15/2020	304L	Seawater	45.1	87.7	Cavernous and small shallow pits
9/2/2020	316L	Seawater	29	55.2	Cavernous and medium-depth pits
9/3/2020	M304B4	Seawater	8.4	11.4	Cavernous and shallow pitting
9/1/2020	M304B4	Seawater	61.7	41.9	Cavernous and shallower groups of pits
8/27/2020	M326	0.1M HCl	3.9	1.1	Strings of shallow pits with some deeper
8/21/2020	M327	0.1M HCl	3.3	1.1	Strings of shallow pits
11/5/2020	304L	0.1M HCl	27.6	60.7	Strings of shallow pits with some deeper
11/5/2020	316L	0.1M HCl	48.7	77.7	Cavernous pits and shallow pits
9/10/2020	M304B5	0.1M HCl	13.7	30.1	Gaping pits with many small, shallow pits
8/27/2020	M304B4	0.1M HCl	53.1	60.8	Cavernous and shallow pits

3.2 Acquisition of neutron-absorbing materials

3.2.1 Borated stainless steels

The powder metallurgy, Grade-A, corrosion samples are available at INL [18]. These materials were developed by the Carpenter Technology Corporation (CarTech) to improve the borated alloy microstructure (boride shape and distribution) and enhance their mechanical properties and corrosion resistance [19-21]. One reference of interest concludes that the corrosion resistance of a Grade-A material (1.75% B) is equivalent to that of a Grade-B material (1.1% B) in 15,000 ppm boric acid with 10 ppm Cl-

Idaho National Laboratory

Neutron Absorber Material Corrosion
Testing Report

Identifier:

Revision: 0

Effective Date: 12/17/2020

Page 44 of 52

at 150°C [21]. Numerous inquiries and requests for Grade-A test materials were made to the CarTech research and marketing groups, without success.

The development of BSS ingot metallurgy began in the 1970s [22]. These ingot metallurgy products were produced and marketed domestically by CarTech, though now their emphasis is on Grade-A, powder metallurgy products. Two commercial sources are available for Grade-B materials: Bohler Bleche GmbH & Co KG and Industeel USA LLC (ArcelorMittal Group). Bohler Bleche (BB) has been in the business of producing these alloys for over 30 years. The BB Neutronit alloy and the major projects it has supported were described in a presentation to the Nuclear Regulatory Commission [23]. Discussions between INL and BB resulted in BB furnishing two sample pieces to INL, as described in Tables 5 and 6 [24].

These heats have a relatively high boron loading (1.25% and 1.27%) that would adversely affect corrosion performance. These materials were not tested in the FY2020 program. Industeel is a wholly owned subsidiary of the ArcelorMittal Group, the world's largest steel production company, and has steel production facilities worldwide. Industeel USA handles products in the U.S. market. Their product designation is NUCL 304B4 [25]. The ArcelorMittal research and development center (Centre de Recherche des Matériaux du Creusot) produces specialty plates, SS, and alloys, located in France. ArcelorMittal recently produced BSS plates for large projects such as the International Thermonuclear Experimental Reactor (Tokamak) fusion project in Southern France.

Table 7. FA 2340348, heat E10729, 610 x 305 x 10 mm.

C	Si	Mn	P	S	Cr	Ni	N	Co	B
0.017	0.30	0.67	0.019	<0.0003	18.49	12.59	0.03	<0.05	1.27

Table 8. FA 2340722, heat E10523, 610 x 305 x 5 mm.

C	Si	Mn	P	S	Cr	Ni	N	Co	B
0.021	0.28	0.62	0.017	<0.0003	18.40	12.54	0.03	<0.05	1.25

Reduced boron content alloy: A lowered-boron-content, Grade-B BSS employing enriched boron in an ingot metallurgy product might be suitable for service [1,26]. The basic concept is to use an addition of enriched boron (50% enrichment at a boron level of 0.5 wt.%) instead of the nominal natural boron level of approximately 1.25 wt.% in order to enhance corrosion resistance and mechanical properties via the ingot metallurgy microstructure. BB and Industeel were approached to see if a small, lab-scale heat with a (natural) boron level of 0.5% could be produced. Neither company expressed an interest.

Idaho National Laboratory

Neutron Absorber Material Corrosion Testing Report	Identifier:
	Revision: 0
	Effective Date: 12/17/2020

Page 45 of 52

3.2.2 Gd+B stainless steels

Powder metallurgy stainless steels with boron and gadolinium additions (SS+Gd+B): Another powder metallurgy product listed by CarTech is CARTECH Micro-Melt DuoSorb 316NU Alloy [27-29]. This material is not covered in any ASTM specification, and was apparently produced in limited quantities. The technical staff at CarTech are presently hoping to locate samples for this program.

Duplex and super-duplex stainless steels with boron and/or gadolinium additions: Duplex (17–22 wt.% Cr) and super duplex (25–27 wt.% Cr) are SSs with a nominal microstructure of 50% austenite and 50% ferrite phases. They have seen extensive use in certain seawater applications [30]. Two recent papers discussed the preparation and corrosion performance of duplex SSs with boron and/or gadolinium additions [31-32]. We requested any available sample materials from the authors but received no reply. The material for these tests was produced under laboratory conditions.

3.2.3 Aluminum composites (Boral)

Boral (an aluminum cermet) was replaced in 2016 by the 3M Advanced Metal Matrix Composite. The material was dropped from the corrosion test program because it was not designed for corrosion resistance in seawater.

3.2.4 Neutron-absorbing, corrosion-resistant coatings

ANA coatings: One proposed use of thermal spray coatings is to provide enhanced neutron-absorption and corrosion-resistance performance to the surfaces of the chevron insert absorber plates [33]. Neutron-absorbing/corrosion-resistant construction materials being considered for this plate are BSS (ingot or powder metallurgy fabrication process) and ANA, both of which are described in the corrosion test plan [1]. Such test conditions (synthetic seawater at 30, 60, and 90°C) are aggressive and could cause high rates of general and localized corrosion (pitting/crevice).

The nominal chevron insert thickness is 3 mm. Assuming that the fabrication process for this component is to cold bend a 3-mm strip product to shape, the ductility of the material must be evaluated. The addition of Gd or B to a corrosion-resistant alloy will decrease ductility with increasing levels of addition. If the amount of B or Gd would need to be reduced in the chosen chevron alloy, a corrosion-resistant/neutron-absorbing coating might make up the difference.

INL recently received approximately 200 lbs of a thermal spray powder that has a base composition of Alloy 22 (UNS NO6022, Ni-Cr-Mo chemistry) with a 2 wt.% addition of gadolinium. This material is similar in chemistry to the M327 heat in Table 1. The material is being procured through Haynes

Idaho National Laboratory

Neutron Absorber Material Corrosion Testing Report	Identifier:
	Revision: 0
	Effective Date: 12/17/2020

Page 46 of 52

International, Kokomo, IN. It will be applied to a 304L substrate by SNL, using the cold spray process. The pieces will then be turned into corrosion samples.

Structurally amorphous materials (SAM): SAM2X5 (15.2% B): Another material that can be considered for coating applications is SAM2X5. Extensive thermal spray process development, along with corrosion testing programs, was conducted by Lawrence Livermore National Laboratory (LLNL) on corrosion-resistant, thermal-neutron-absorbing, iron-based amorphous alloys, with some favorable results [34-36]. This material was initially developed by NanoSteel Company, Inc. The rights were assigned to the Lincoln Electric Company, and this material is now designated as SHS 7574 HVOF.

3.2.5 Summary of NAM options

- The demand for highly corrosion resistant, neutron-absorbing materials is essentially non-existent. The ANA development program ended with the closure of the National Spent Nuclear Fuel Program (NSNFP) at INL. If additional test material is deemed necessary, a supply chain for this material would have to be developed. Another factor is the effect of the pandemic on U.S. nickel-based-alloy suppliers. This has resulted in the reduced sale of high-temperature aerospace alloys by possible ANA producers such as Haynes International and Special Metals Corporation, which could affect the willingness of these and other suppliers to work with INL/DOE on the development of production methods for ANA materials.
- The ingot metallurgy BSSs are available from two European mills, with no known U.S. suppliers. CarTech is not, at present, in production of their powder metallurgy, borated, and boron/gadolinium alloys.
- SAM2X5 thermal spray powder is currently available from Lincoln Electric as SHS 7574 HVOF. An ANA powder product for thermal spray application is presently available from Haynes International.
- Technology for producing coatings and bulk materials has advanced in the past decade, providing opportunities to produce unique materials, including grading the composition to optimize corrosion performance for exposed surfaces and co-spraying different powders of different chemistries.

Neutron Absorber Material Corrosion Testing Report	Identifier: Revision: 0 Effective Date: 12/17/2020
---	--

Identifier: Revision: 0 Effective Date: 12/17/2020	Page 47 of 52
--	---------------

4. Observations

General:

- In each environment, the general corrosion rates were similar for all specimens, with acceptable general corrosion rates for 0.028 M NaCl and seawater, while several orders of magnitude greater in 0.1 M HCl. Alloy 22 showed low rates in all environments.
- All alloys other than Alloy 22 appear susceptible to pitting corrosion, as evidenced by CPP measurements with close or overlapping E_{corr} and E_{rp} values.
- No significant difference in general corrosion was observed between seawater and 0.028 M NaCl, while general corrosion rates orders of magnitude greater were observed for 0.1 M HCl.
- In all environments, the pit depths were significantly greater for SS specimens compared to ANA.
- In more aggressive 0.1 M HCl, the ANA specimen becomes significantly more resistant than the SS alloys, particularly M327 (higher-Cr version).

Borated SS:

- There was no significant difference in corrosion properties between the two BSS alloys and the benchmark SS specimens. It appears that, for lower B specimens tested in this work, the base alloy can be considered a close analog. Given that 304L is not deemed suitable for seawater use, it follows that BSS should not be suitable, particularly for the long duration involved in the application.
- Note that while the BSS specimens are based off 304 composition, there is greater chromium and significantly greater nickel (than 304L or 316L) with powder metallurgy possibly playing a role in bringing performance close to 304L levels.
- No significant difference was observed between the two BSS alloys in terms of both general corrosion rates and CPP parameters, whereas, in some cases, 304B5 showed slightly better values.

ANA:

- It is challenging to compare ANA corrosion due to the localized dissolution of the secondary phase. In the CPP tests, polished specimens show significant current in the passive region.
- For pickled specimens, when the exposed secondary phase has been dissolved, CPP curves and general corrosion rates improve and show similarity to Alloy 22 in harsh 0.1 M HCl.

Idaho National Laboratory**Neutron Absorber Material Corrosion Testing Report**

Identifier:

Revision: 0

Effective Date: 12/17/2020

Page 48 of 52

- More work is needed to assess if the secondary phase is distributed enough to limit deeper penetration. Alloy performance could be tied to microstructure, which is influenced at various steps in the manufacturing process.

5. Testing activities for FY21

Future activities are planned to broaden the material palette to include specimens produced via advanced manufacturing practices. These activities will be captured in a test plan to be produced in the near future. New work will include alloys, coatings and 3-D printed materials. Coated specimens will be tested using a slightly different cell designed to seal to one side of a flat specimen. While the search for new BSS materials has not been fruitful, the search for materials containing boron will continue.

5.1 New alloy testing

- ORNL 3-D printed specimen corrosion testing, BSS, BSS with 316L outer layers, ANA and Alloy 22
- Duplex and super-duplex SSs and more highly alloyed austenitic SSs have a long history of use in components for seawater service. Research papers discussed earlier show that B and Gd can be added to these duplex alloys [31-32]. A literature review should be conducted to see how these alloys (without B or Gd additions) might be suitable for our test conditions.

5.2 NAM coatings

- SNL is developing coating parameters and will fabricate corrosion coupons using an ANA powder (Alloy 22 with 2-wt.% Gd). These coupons should be added to the corrosion test program.
- Corrosion coupons should be prepared with Alloy 22 powder (via the same process and parameters as used for the ANA powder application) and tested for baseline data comparison purposes.
- SAM2X5 coating testing. Subject matter experts in the thermal spray process (powder feedstock application) should evaluate the proper process for applying this material to corrosion coupons and/or chevron inserts. The LLNL program used both high-velocity oxygen fuel and high-velocity air fuel. Based on their findings, the program will obtain SAM2X5 powder and have corrosion coupons prepared according to the recommended process. These coupons should be included in the 2021 corrosion test program.
- Examine possibility of producing thermal spray coatings consisting of boron carbide powder co-sprayed with Alloy 22 powder.
- Test ANA material with a thermally spray coating of Alloy 22 onto ANA substrate to assess overall corrosion performance and loss of Gd from the material.

Idaho National Laboratory

Neutron Absorber Material Corrosion Testing Report	Identifier:
	Revision: 0
	Effective Date: 12/17/2020

Page 49 of 52

5.3. Follow-on corrosion testing to support FY20 testing

- ANA surface-condition corrosion testing. Corrosion testing with the ANA material shows that the dissolution of the gadolinide (Ni_5Gd) phases that intersect the surface results in a higher initial corrosion current that slowly fades away over time. This work has already started with preliminary work reported here.
- Perform additional tests to clear up any remaining questions from FY20 testing.
- Include other electrochemical methods such as potentiostatic testing, where the specimen is held at a potential at or near E_{corr} and current is measured versus time.

References

- 1) INL PLN 6095, *Neutron Absorber Material Test Plan*, INL/EXT-20-58534, 2020.
- 2) V. Jain, S. D. Sevougian, P. D. Mattie, K. G. Mon, and R. J. Mackinnon, *Implementation of Localized Corrosion in the Performance Assessment Model for Yucca Mountain*. United States: N. p., 2006. Web. Conference: 2006 International High-Level Radioactive Waste Management Conference, Las Vegas, Nevada, April 30-May 4, 2006.
- 3) G. S. Frankel, *Pitting Corrosion of Metals: A Review of the Critical Factors*, Journal of the Electrochemical Society **145** (1998) 2186.
- 4) R. B. Rebak, *Factors Affecting the Crevice Corrosion Susceptibility of Alloy 22*, NACE Corrosion 2005, Paper 05610, Houston, TX, 2005.
- 5) ASTM G59 – 97 (Reapproved 2014), *Conducting Potentiodynamic Polarization Resistance Measurements*, ASTM International, West Conshohocken, PA.
- 6) Hardin, E. 2019. Technical Memo on Neutron Absorber Materials. Milestone M5SF-19SN020403023. Albuquerque, NM: Sandia National Laboratory.
- 7) T. E. Lister, R. E. Mizia, A. Erickson, Tammy Trowbridge, *Electrochemical Corrosion Testing of Neutron Absorber Materials*, INL/EXT-06-11772, 2007.
- 8) ASTM D1141 – 99 (2013) *Standard Practice for the Preparation of Substitute Ocean Water*, ASTM International, West Conshohocken, PA.
- 9) D. S. Dunn, O. Pensado, Y.-M. Pan, R. T. Pabalan, L. Yang, X. He, K. T. Chiang, *Passive and Localized Corrosion of Alloy 22 — Modeling and Experiments*, CNWRA 2005-02 U.S. Nuclear Regulatory Commission Contract NRC-02-02-012, 2005.
- 10) R. B. Rebak, Selection of Corrosion Resistant Materials for Nuclear Waste Repositories, Materials Science and Technology (2006) (MOL—200610260049)
- 11) R. E. Mizia, T. E. Lister, P. J. Pinhero, *Microstructure and Corrosion Performance of a Neutron Absorbing Ni-Cr-Mo-Gd Alloy*, NACE Corrosion 2003, Paper 03679.
- 12) ASTM G5 – 14 (2014) *Standard Reference Test Method for Making Potentiodynamic Anodic Polarization Measurements*, ASTM International, West Conshohocken, PA.
- 13) ASTM G102 – 89 (2015) *Standard Practice for Calculation of Corrosion Rates and Related Information from Electrochemical Measurements*, ASTM International, West Conshohocken, PA.

Idaho National Laboratory

Neutron Absorber Material Corrosion Testing Report	Identifier:
	Revision: 0
	Effective Date: 12/17/2020

Page 50 of 52

- 14) R. C. Pistorius, *The Effect of Some Fundamental Aspects of the Pitting Corrosion of Stainless Steel on Electrochemical Noise Measurements, Electrochemical Noise Measurement for Corrosion Applications*, ASTM STP 1277, American Society for Testing and Materials, 1996, pp. 343-358.
- 15) R. M. Kain, *Crevice Corrosion Behavior of Stainless Steel in Seawater and Related Environments*, *Corrosion* **40** (1984) 313.
- 16) R. E. Mizia and T. E. Lister, *Accelerated Testing of Neutron-Absorbing Alloys for Nuclear Criticality Control*, *Nuclear Technology* **176** (2011) 9.
- 17) T. E. Lister, R. E. Mizia, A. W. Erickson, B. S. Matteson, *General and Localized Corrosion of Borated Stainless Steels*, NACE Corrosion 2008, Paper 08590, New Orleans, LA, 2008.
- 18) ASTM A 887-89 (2014) *Standard Specification for Borated Stainless Steel Plate, Sheet, and Strip for Nuclear Application*, ASTM International, West Conshohocken, PA.
- 19) J. W. Martin, *Effects of Processing and Microstructure on the Mechanical Properties of Boron-Containing Austenitic Stainless Steels*, Proceedings of the Symposium on Waste Management, University of Arizona, Tucson, AZ, 1989.
- 20) Carpenter Technology Corporation Datasheet, *CarTech Micro-Melt NeutroSorb Plus Alloys*, Date 03/04/09.
- 21) R. S. Brown, (CarTech), *Corrosion Resistance of Borated Stainless Steels Carpenter Neutrosorb Plus (Grade A) and Neutrosorb (Grade B)*, CarTech Internal Research Reports, 03/28/91.
- 22) H. J. Goldschmidt, *Effect of Boron in 18% Cr, 25% Ni Austenitic Steel*, The Journal of the Iron and Steel Institute, Nov. 1971.
- 23) A. Presti, *Shielding Materials for Nuclear Industry*, NRC Meeting – NAMs, March 14, 2013.
- 24) Email, Jeremy Steinman (Bohler Bleche) to Ronald Mizia (SNF Project), March 30, 2020.
- 25) Industeel/Arcelor Mittal NUCL 304B4, dated 12/2019.
- 26) H. Ha, J. H. Jang, T. Lee, C. Won, C. Lee, J. Moon, and C. Lee, *Investigation of the Localized Corrosion and Passive Behavior of Type 304 Stainless Steels with 0.2–1.8 wt % B*, *Materials* **11** (2018) 2097.
- 27) Carpenter Technology Corporation Datasheet, *CarTech Micro-Melt DuoSorb 316NU Alloys, Edition D Date 1/20/2016*.
- 28) M. L. Schmidt, G. J. Del Corso, K. A. Klankowski, L. W. Lherbier, and D. J. Novotnak, *Review of the Development and Testing of a New Family of Boron and Gadolinium-Bearing Dual Thermal Neutron Absorbing Alloys*, Waste Management 2013 Conference, Feb. 24–28, Phoenix, AZ, 2013.
- 29) United States Patent, Patent Number: US9,267,192 B2, Michael L. Schmidt, Gregory J. Del Corso, Patrick C. Ray, Ning Ma, *Processable High Thermal Neutron Absorbing Fe-Base Alloy Powder*, Feb. 23, 2016.
- 30) B. Wallen, *Corrosion of Duplex Stainless Steels in Seawater*, Duplex Stainless Steels 97: 5th World Conference [organized by: Stainless Steel World. Fifth World Conference on Duplex Stainless Steels, Maastricht, the Netherlands, 21-23 October 1997].
- 31) Y. Choi, B. M. Moon, D. S. Song, *Fabrication of Gd Containing Duplex Stainless Steel Sheet for Neutron Absorbing Structural Materials*, *Nuclear Engineering and Technology* **45** (2013) 689-694.

Idaho National Laboratory

Neutron Absorber Material Corrosion Testing Report	Identifier:
	Revision: 0
	Effective Date: 12/17/2020

Page 51 of 52

32) M. Jung, Y. Baik, Y. Choi, and D. S. Sohn, *Corrosion and Mechanical Properties of Hot-Rolled 0.5%Gd-0.8%B Stainless Steels in a Simulated Nuclear Waste Treatment Solution*, Nuclear Engineering and Technology **51** (2019) 207-213.

33) Options for Future Fuel/Basket Modifications for DPC Disposition, Section 2.2, Sandia National Laboratories, Albuquerque, NM, M4SF-20SN010305051, Rev. 1, June 2020.

34) P. D. Hailey, J. C., Farmer, S. D. Day, and R. B. Rebak, *Anodic Behavior of SAM2X5 Material Applied as Amorphous Coatings*, Materials Science and Technology, Detroit, MI, Sept. 16-20, 2007, UCRL-CONF-233635.

35) J. C. Farmer, J. S. Choi, C. K. Saw, R. Rebak, S. D. Day, T. Lian, P. Hailey, J. H. Payer, D. J. Branagan, and L. F. Aprigliano, *Corrosion Resistance of Amorphous $Fe_{49.7}Cr_{17.7}Mn_{1.9}Mo_{7.4}W_{1.6}B_{15.2}C_{3.8}Si_{2.4}$ Coating: A New Criticality Control Material*, Nuclear Technology **161** (2008) 169-189, DOI:10.13182/NT08-A3921.

36) J. Blink, J. Farmer, J. Choi, and S. Saw, *Applications in the Nuclear Industry for Thermal Spray Amorphous Metal and Ceramic Coatings*, Metallurgical and Materials Transactions A, 1344-Volume 40A, June 2009.